

An Allen–Cahn approach to the remodelling of fibre-reinforced anisotropic materials

Original

An Allen–Cahn approach to the remodelling of fibre-reinforced anisotropic materials / Grillo, Alfio; Carfanga, Melania; Federico, Salvatore. - In: JOURNAL OF ENGINEERING MATHEMATICS. - ISSN 0022-0833. - STAMPA. - 109:1(2018), pp. 139-172. [10.1007/s10665-017-9940-8]

Availability:

This version is available at: 11583/2683512 since: 2020-06-02T19:45:07Z

Publisher:

Springer

Published

DOI:10.1007/s10665-017-9940-8

Terms of use:

This article is made available under terms and conditions as specified in the corresponding bibliographic description in the repository

Publisher copyright

Springer postprint/Author's Accepted Manuscript

This version of the article has been accepted for publication, after peer review (when applicable) and is subject to Springer Nature's AM terms of use, but is not the Version of Record and does not reflect post-acceptance improvements, or any corrections. The Version of Record is available online at: <http://dx.doi.org/10.1007/s10665-017-9940-8>

(Article begins on next page)

1 An Allen-Cahn Approach to the Remodelling 2 of Fibre-Reinforced Anisotropic Materials

3 Alfio Grillo · Melania Carfagna ·
4 Salvatore Federico

5
6 Received: date / Accepted: date

7 **Abstract** We propose a theory of remodelling in fibre-reinforced biological
8 tissues, in which the fibre orientation follows a given probability density. The
9 latter is characterised by variance and mean angle. We claim that the fibres
10 may change their orientation in time, thereby triggering a remodelling process
11 that can be described by the spatiotemporal evolution of the mean angle.
12 This is determined by solving a balance of external and internal generalised
13 forces. We assign the latter ones by establishing a constitutive theory capable
14 of resolving the spatial variability of the fibre mean angle, and featuring a
15 free energy density of the Allen-Cahn type. Through numerical simulations,
16 we compare the predictions of our model with the results of another model
17 available in the literature. Finally, we interpret the evolution of the mean angle
18 as the consequence of a symmetry breaking that occurs in the tissue both
19 spontaneously and due to the coupling between remodelling and deformation.

20 **Keywords** Porous Media · Biological tissue · Biphasic material · Fibre-
21 reinforcement · Transverse isotropy · Remodelling · Structural changes

This work has been supported in part by the *Politecnico di Torino* (Italy) [AG and MC], in part by the *Fondazione Cassa di Risparmio di Torino* (Italy), through the *La Ricerca dei Talenti* (“HR Excellence in Research”) programme [AG and MC] and in part by the Natural Sciences and Engineering Research Council of Canada, through the NSERC Discovery Programme [SF].

A. Grillo (Corresponding Author) · M. Carfagna
Dept of Mathematical Sciences (DISMA) “G.L. Lagrange”, Politecnico di Torino
Corso Duca degli Abruzzi 24, 10129, Torino, Italy
Tel.: +39-011-0907531. Fax: +39-011-0907599
E-mail: alfio.grillo@polito.it
E-mail: melania.carfagna@polito.it

S. Federico
Dept of Mechanical and Manufacturing Engineering, The University of Calgary
2500 University Drive NW, Calgary, AB, T2N 1N4, Canada
E-mail: salvatore.federico@ucalgary.ca

1 Introduction

Following Cowin's terminology [1], a biological tissue is “*a collection of cells*” embedded in an extracellular matrix (ECM). Among the constituents of the ECM, elastin and collagen fibres play an essential role in determining the mechanical properties of tissues.

In order to understand how a tissue is generated, how it works, and how it adapts itself to external stimuli, it is necessary to know the internal structure of the tissue itself and the mechanical behaviour of its constituents. Of particular relevance is the study of the ECM, whose properties are tightly related to the presence of elastin and collagen fibres, and to their spatial orientation. In the case of blood vessels, several mathematical models of the tissue's mechanics have been elaborated, in which a discrete number of families of fibres is considered (see, e.g., [2–6]). Moreover, models that consider statistically oriented fibres have been proposed for various tissues, for example, in [7–10]. To account for the fibres in the constitutive description of biological tissues, the structure tensor is included in the determination of stress through the introduction of suitable invariants of the Cauchy deformation tensor [2, 11, 12].

When the ECM is permeated by an interstitial fluid, the pattern of fibre orientation influences the motion of the fluid by either facilitating or hindering its flow. For instance, this is the case of articular cartilage, whose permeability in the superficial zone should be higher than it actually is, based solely on considerations on the proteoglycan volumetric fraction, as observed by Maroudas and Bullough [13]. Maroudas and Bullough [13] also inferred that this behaviour was likely due to the collagen fibres, which, in the superficial zone, are oriented parallel to the surface and therefore constitute a further obstacle to fluid flow. A possible explanation of this occurrence has been presented in [9]. Subsequently, by putting together the non-linear elasticity model presented in [14], and extending to large deformations the permeability model developed in [15], a general, finite-deformation model was introduced in [16]. In this series of papers, the fibres are assumed to be oriented statistically according to a probability density capable of mimicking the histological pattern observed by other authors [17, 18].

When a tissue deforms, its mechanical properties evolve in time. The deformation, indeed, drives the reorientation of the fibres, thereby modulating the mechanical behaviour of the tissue also in response to the changes in its internal structure. If the deformation is the only responsible for this structural reorganisation, the evolution of the fibre pattern may be said to be a *passive consequence* of the deformation. If, however, as suggested in [19], a tissue is supposed to possess also structural degrees of freedom, which exist independently of deformation, then the reorientation of the fibres becomes part of the tissue dynamics, and it *interacts* with the deformation and stress. This interaction, in turn, may manifest itself in several ways, among which a relevant one is given by the identification of a *stress-driven* pattern of fibre arrangement.

Motivated by the aforementioned considerations, the scope of this work is to propose a model of structural adaptation in fibre-reinforced biological

67 tissues. In the present framework, the “structural adaptation” is assumed to
68 consist of a variation of the material properties that determine the local ori-
69 entation of the fibres in a fibre-reinforced soft tissue [20,21]. More specifically,
70 we consider a simplified theoretical setting, in which the only interactions ex-
71 perience by the tissue arise due to mechanical stimuli, and the tissue itself is
72 hyperelastic. Moreover, no inelastic distortions are considered. Hence, the re-
73 orientation of fibres is assumed not to be accompanied by growth, resorption,
74 or any other process of this kind. Still, dissipative entities yielding the vari-
75 ation of the tissue’s internal structure are taken into account. Following the
76 line of thought put forward in [22,23], a probability distribution of the fibre
77 orientation is prescribed, whose functional law features a family of parameters
78 depending on the material points and on time. These parameters shall be re-
79 ferred to as *remodelling variables* in the sequel. While the dependence of the
80 remodelling variables on the material points is related to the inhomogeneity
81 of the tissue, their dependence on time is introduced here in order to allow for
82 their evolution, which is understood as a manifestation of the tissue’s struc-
83 tural adaptation. On this footing, we present a theory of remodelling that,
84 starting from the setup outlined in [22,23], relies on the introduction of a free
85 energy density of the Ginzburg-Landau [24,25] or Allen-Cahn [26] type, and
86 accounts explicitly for the spatial resolution of the remodelling variable¹.

87 As done in [27,22,23], the hypothesis is made that the remodelling vari-
88 ables are indeed “kinematic variables”, for which suitable balance laws should
89 be introduced in conjunction with the balance laws typically adopted in the
90 continuum mechanics of simple bodies. In this respect, this vision of structural
91 adaptation takes large inspiration from the models of Cermelli et al. [28] and
92 DiCarlo and Quiligotti [19], in which the concept of a “two-layer dynamics” is
93 thoroughly explained.

94 Previous studies on remodelling have been conducted by many other au-
95 thors. For example, the interplay between the fibre alignment in fibre-reinforced
96 media and other aspects of the tissue mechanics has been highlighted in [29],
97 while remodelling in collagen gels and tissues with collagenous reinforcement
98 has been studied in [30]. In a slightly different context, a possible coupling
99 between fibre reorientation and growth has been proposed in [31], in conjunc-
100 tion with the Bilby-Kröner-Lee decomposition. Furthermore, the remodelling
101 of the collagen fibres has been addressed also in [32], and the compaction of
102 collagen gels has been studied in [33]. Recently, the influence of the collagen
103 fibres on the mechanics of the aorta has been studied in [34–36].

104 The remainder of this work is organised as follows. In Section 2, we intro-
105 duce the dynamics of remodelling. In Section 3, we establish the constitutive
106 framework. In Section 4, we study in detail the remodelling equation, and dis-
107 cuss its asymptotic behaviour. In Section 5, we comment the results of the
108 numerical simulations. Finally, in Section 6, we summarise the key-points of
109 our work, and propose an outline for future research.

¹ The idea was suggested by Prof. Gaetano Giaquinta to S. Federico, S.-K. Han, and A. Grillo during the visit of S.-K. Han to the University of Catania, in 2004, while discussing about the histology of articular cartilage.

110 2 General mathematical model

111 We consider a fibre-reinforced porous medium, in which the reinforcing fibres
 112 are oriented statistically according to some suitable probability density. To
 113 formalise the mathematical description of media of this type, we refer to the
 114 works [37, 16, 38–40], which we briefly summarise here. Within the present
 115 theoretical framework, the tissue is regarded as a biphasic medium comprising
 116 a fluid and a solid phase. The solid phase is the representation of a porous
 117 medium, which is assumed to consist of a matrix of biological polymers (e.g.,
 118 proteoglycans in the case of articular cartilage) and a network of collagen
 119 fibres.

120 2.1 Theoretical background

121 At the scale at which our theory is formulated, the matrix and the collagen
 122 fibres constitute a mixture, in which they are present with volumetric fractions
 123 ϕ_{0s} and ϕ_{1s} , respectively. The sum $\phi_s = \phi_{0s} + \phi_{1s}$ defines the volumetric fraction
 124 of the solid phase as a whole and, since the saturation condition is assumed
 125 to apply, the volumetric fraction of the fluid phase coincides with the porosity
 126 of the medium and is given by $\phi_f = 1 - \phi_s$.

127 The portion of the three-dimensional Euclidean space, \mathcal{S} , occupied by the
 128 tissue at time t is said to be the *current configuration* of the tissue. We also
 129 introduce a reference configuration, \mathcal{B} . For $x \in \mathcal{S}$ and $X \in \mathcal{B}$, we consider
 130 the tangent spaces $T_x\mathcal{S}$ and $T_X\mathcal{B}$, and the co-tangent spaces $T_x^*\mathcal{S}$ and $T_X^*\mathcal{B}$.
 131 Moreover, we denote by $T\mathcal{S} = \sqcup_{x \in \mathcal{S}} T_x\mathcal{S}$ and $T\mathcal{B} = \sqcup_{X \in \mathcal{B}} T_X\mathcal{B}$ the tangent
 132 bundles of \mathcal{S} and \mathcal{B} , and by $T^*\mathcal{S} = \sqcup_{x \in \mathcal{S}} T_x^*\mathcal{S}$ and $T^*\mathcal{B} = \sqcup_{X \in \mathcal{B}} T_X^*\mathcal{B}$ their
 133 co-tangent bundles, respectively [41]. Finally, the space \mathcal{S} and the reference
 134 configuration \mathcal{B} are endowed with the metric tensors \mathbf{g} and \mathbf{G} , respectively.

135 In the present framework, matrix and fibres are assumed to share the same
 136 motion. This hypothesis allows to describe the motion of the solid phase by
 137 means of a one-parameter family of smooth embeddings. At each time t , the
 138 embedding $\chi(\cdot, t)$ maps the points of \mathcal{B} into \mathcal{S} (see [37, 38] for details), i.e.,

$$\chi(\cdot, t) : \mathcal{B} \rightarrow \mathcal{S}, \quad X \in \mathcal{B} \mapsto x = \chi(X, t) \in \mathcal{S}. \quad (1)$$

139 The tangent map $T\chi(X, t) = \mathbf{F}(X, t) : T_X\mathcal{B} \rightarrow T_{\chi(X, t)}\mathcal{S}$ is the deformation
 140 gradient tensor of the solid phase [41], while $\mathbf{C} = \mathbf{F}^T \mathbf{g} \mathbf{F}$ and $\mathbf{b} = \mathbf{F} \mathbf{G}^{-1} \mathbf{F}^T$
 141 denote the right and the left Cauchy-Green deformation tensor, respectively. In
 142 order for $\chi(X, t)$ to be admissible, $\mathbf{F}(X, t)$ is required to have strictly positive
 143 determinant, $J(X, t) = \det \mathbf{F}(X, t)$, at all points and at all times.

144 To complete the kinematic description of the considered porous medium,
 145 we introduce the velocities of the solid and fluid phase, \mathbf{v}_s and \mathbf{v}_f , the *filtration*
 146 *velocity* $\mathbf{q} = \phi_f \mathbf{w}$, with $\mathbf{w} = \mathbf{v}_f - \mathbf{v}_s$ being the relative velocity of the fluid
 147 with respect to the solid motion, and the backward Piola transformation of \mathbf{q} ,
 148 $\mathbf{Q} = J \mathbf{F}^{-1} \mathbf{q}$, which is referred to as the *material* filtration velocity.

149 2.2 Directional averages

150 At the scale of a single fibre, the fibre appears as a curved cylinder whose
 151 length is much larger than the diameter of the cross section. This allows to
 152 model the fibre as a curve. Furthermore, in a sufficiently small neighbourhood
 153 of a given point $X \in \mathcal{B}$, a fibre can be approximated by its tangent line [15],
 154 which defines the local direction of fibre alignment. Such direction can be
 155 associated with a unit vector, \mathbf{M}_X , emanating from X . Since the orientation
 156 of the fibres is assumed to be statistical at each point, we need to define
 157 the probability density that a fibre passing by X is oriented along a given
 158 direction. To this end, we introduce the set of all unit vectors of $T_X\mathcal{B}$, i.e.,
 159 $\mathbb{S}_X^2\mathcal{B} = \{\mathbf{M}_X \in T_X\mathcal{B} : \|\mathbf{M}_X\| = 1\}$, and the function $\Psi_X : \mathbb{S}_X^2\mathcal{B} \rightarrow \mathbb{R}_0^+$
 160 such that, for a given $\mathbf{M}_X \in \mathbb{S}_X^2\mathcal{B}$, $\Psi_X(\mathbf{M}_X)$ is the probability density that
 161 a (rectified) fibre passing from X is locally aligned along \mathbf{M}_X . Since Ψ_X is
 162 assumed to be a continuous probability density, it has to be normalised.

163 Given a physical property (e.g., a scalar one) depending on the direction of
 164 the fibres at X , and expressed thus as $\mathfrak{F}_X : \mathbb{S}_X^2\mathcal{B} \rightarrow \mathbb{R}$, the *directional average*
 165 of \mathfrak{F}_X is defined by (see, e.g., [16] and references therein)

$$\begin{aligned} \langle\langle \mathfrak{F}_X \rangle\rangle &= \int_{\mathbb{S}_X^2\mathcal{B}} \mathfrak{F}_X(\mathbf{M}_X) \Psi_X(\mathbf{M}_X) \\ &= \int_0^{2\pi} \int_0^\pi \mathfrak{F}_X(\hat{\mathbf{M}}_X(\theta, \phi)) \Psi_X(\hat{\mathbf{M}}_X(\theta, \phi)) \sin(\theta) d\theta d\phi, \end{aligned} \quad (2)$$

166 where, for $(\theta, \phi) \in [0, \pi] \times [0, 2\pi[$,

$$\mathbf{M}_X = \hat{\mathbf{M}}_X(\theta, \phi) = \sin \theta \cos \phi \mathbf{e}_1 + \sin \theta \sin \phi \mathbf{e}_2 + \cos \theta \mathbf{e}_3, \quad (3)$$

167 and $\{\mathbf{e}_I\}_{I=1}^3$ is an orthonormal vector basis of $T_X\mathcal{B}$. The second equality in
 168 (2) stems from rephrasing the integral over $\mathbb{S}_X^2\mathcal{B}$ as a surface integral and ex-
 169 pressing it in spherical coordinates, granted that each $\mathbf{M}_X \in \mathbb{S}_X^2\mathcal{B}$ corresponds
 170 univocally to a point on the surface of the unit sphere centred at X .

171 In this work, we assume that the matrix of the solid phase is isotropic and
 172 that a fibre aligned along \mathbf{M}_X at $X \in \mathcal{B}$ is transversely isotropic with respect
 173 \mathbf{M}_X . Thus, \mathfrak{F}_X must satisfy the symmetry condition $\mathfrak{F}_X(\mathbf{H}\mathbf{M}_X) = \mathfrak{F}_X(\mathbf{M}_X)$,
 174 for all proper rotation tensors \mathbf{H} such that $\mathbf{H}\mathbf{M}_X = \pm\mathbf{M}_X$. If there exists a
 175 direction of symmetry for the whole tissue, i.e., if there exists \mathbf{M}_0 such that
 176 for all $X \in \mathcal{B}$, for all $\mathbf{M}_X \in \mathbb{S}_X^2\mathcal{B}$, and for every proper rotation tensor \mathbf{H}_0
 177 with the property $\mathbf{H}_0\mathbf{M}_0 = \pm\mathbf{M}_0$, the invariance condition $\Psi_X(\mathbf{H}_0\mathbf{M}_X) =$
 178 $\Psi_X(\mathbf{M}_X)$ holds true, then the probability density is transversely isotropic
 179 with respect to \mathbf{M}_0 . Consequently, the directional average $\langle\langle \mathfrak{F}_X \rangle\rangle$ turns out to
 180 be transversely isotropic with respect to \mathbf{M}_0 , while $\mathfrak{F}_X(\mathbf{M}_X)$ is transversely
 181 isotropic with respect to \mathbf{M}_X . Further restrictions descend from the hypothesis
 182 that the physical quantities depending on the orientation of the fibres are
 183 invariant under the transformation $\mathbf{M}_X \mapsto -\mathbf{M}_X$, for all \mathbf{M}_X and for all
 184 $X \in \mathcal{B}$. To fulfil this property, the generic physical quantity \mathfrak{F}_X has to depend
 185 on \mathbf{M}_X through $\mathbf{A}_X = \mathbf{M}_X \otimes \mathbf{M}_X$, which is referred to as *structure tensor*,

186 and fulfils the identity $\mathbf{H}\mathbf{A}_X\mathbf{H}^T = \mathbf{A}_X$. Accordingly, the probability density
 187 must comply with the invariance condition $\Psi_X(\mathbf{M}_X) = \Psi_X(-\mathbf{M}_X)$.

188 When $\mathbf{M}_X \in \mathbb{S}_X^2\mathcal{B}$ is expressed as in (3), the transverse isotropy of Ψ_X
 189 implies that $\Psi_X(\hat{\mathbf{M}}_X(\Theta, \Phi))$ is independent of Φ , whence the possibility of in-
 190 troducing a function $\wp_X: [0, \pi] \rightarrow \mathbb{R}_0^+$ such that $\wp_X(\Theta) = \Psi_X(\hat{\mathbf{M}}_X(\Theta, \Phi))$, for
 191 all $\Phi \in [0, 2\pi[$. To be compatible with the restriction $\Psi_X(\mathbf{M}_X) = \Psi_X(-\mathbf{M}_X)$,
 192 \wp_X must respect the constraint $\wp_X(\Theta) = \wp_X(\pi - \Theta)$, for all $\Theta \in [0, \pi]$. This
 193 property is also satisfied by all the physical quantities studied in this work,
 194 and allows thus to determine the directional averages in (2) by computing the
 195 integrals over the hemisphere $\mathbb{S}_X^{2+}\mathcal{B} = \{\mathbf{M}_X \in \mathbb{S}_X^2\mathcal{B} \mid \mathbf{M}_X \cdot \mathbf{M}_0 \geq 0\}$, i.e.,

$$\begin{aligned} \langle\langle \mathfrak{F}_X \rangle\rangle &= 2 \int_{\mathbb{S}_X^{2+}\mathcal{B}} \mathfrak{F}_X(\mathbf{M}_X) \Psi_X(\mathbf{M}_X) \\ &= \int_0^{2\pi} \int_0^{\pi/2} \mathfrak{F}_X(\hat{\mathbf{M}}_X(\Theta, \Phi)) \bar{\wp}_X(\Theta) \sin(\Theta) d\Theta d\Phi, \end{aligned} \quad (4)$$

196 where $\bar{\wp}_X: [0, \pi/2] \rightarrow \mathbb{R}_0^+$ is a re-definition of \wp_X . Very often, the von Mises
 197 probability density is used when spherical data are concerned [8, 10, 38]. Here,
 198 however, for our purposes, we employ the pseudo-Gaussian density

$$\bar{\wp}_X(\Theta) = \frac{\gamma_X(\Theta)}{2\pi \int_0^{\pi/2} \gamma_X(\Theta') \sin(\Theta') d\Theta'}, \quad (5a)$$

$$\gamma_X(\Theta) = \exp\left(-\frac{[\Theta - Q(X)]^2}{2[\omega(X)]^2}\right), \quad (5b)$$

199 where $Q(X)$ and $[\omega(X)]^2$ represent the mean angle and variance of the prob-
 200 ability density, respectively. The choice of the pseudo-Gaussian distribution is
 201 corroborated by the fact that it modelled satisfactorily the orientation of the
 202 collagen fibres in articular cartilage [9], as determined in the X-ray diffraction
 203 experiments carried out in [18].

204 With a slight abuse of terminology, we call $\mathbb{S}_X^2\mathcal{B}$ *unit sphere* attached at
 205 X and, in analogy with the definition of $T\mathcal{B}$, we call *bundle of unit spheres*
 206 the set $\mathbb{S}^2\mathcal{B} = \sqcup_{X \in \mathcal{B}} \mathbb{S}_X^2\mathcal{B}$. When the point $X \in \mathcal{B}$ is not specified, we adopt
 207 the notation $\Psi: \mathbb{S}^2\mathcal{B} \rightarrow \mathbb{R}_0^+$ and $\mathfrak{F}: \mathbb{S}^2\mathcal{B} \rightarrow \mathbb{R}$, thereby defining both Ψ and
 208 \mathfrak{F} over $\mathbb{S}^2\mathcal{B}$. In this case, we introduce the vector field $\mathbf{M}: \mathcal{B} \rightarrow \mathbb{S}^2\mathcal{B}$ such
 209 that $\mathbf{M}(X) = \mathbf{M}_X \in \mathbb{S}_X^2\mathcal{B} \subset \mathbb{S}^2\mathcal{B}$, and we set $\Psi(\mathbf{M}(X)) = \Psi_X(\mathbf{M}_X)$ and
 210 $\mathfrak{F}(\mathbf{M}(X)) = \mathfrak{F}_X(\mathbf{M}_X)$. Hence, we denote the directional average of \mathfrak{F} by

$$\langle\langle \mathfrak{F} \rangle\rangle := \int_{\mathbb{S}^2\mathcal{B}} \Psi(\mathbf{M}) \mathfrak{F}(\mathbf{M}), \quad (6)$$

211 with the understanding that, when $\langle\langle \mathfrak{F} \rangle\rangle$ is evaluated at $X \in \mathcal{B}$, one obtains
 212 $\langle\langle \mathfrak{F} \rangle\rangle(X) = \langle\langle \mathfrak{F}_X \rangle\rangle$. Sometimes, since \mathfrak{F} depends on the fibre orientation through
 213 the structure tensor, we also use the notation $\langle\langle \mathfrak{F}(\mathbf{A}) \rangle\rangle = \langle\langle \mathfrak{F} \rangle\rangle$.

214 2.3 Dynamics

215 From this point onwards, we employ the symbols “Grad” and “Div” for the
 216 gradient and divergence operators in the reference configuration (or, more
 217 generally, the body manifold) \mathcal{B} , and the symbols “grad” and “div” for the
 218 gradient and divergence operators in the physical space \mathcal{S} . This notation is
 219 standard in modern Continuum Mechanics (e.g. [41]) and allows us to be
 220 consistent with our previous works, to which we constantly make reference
 221 (for some remarks about the notation used in this work, see Appendix A).

222 We formulate the dynamics of the considered system under the hypoth-
 223 esis that its constituents (e.g., matrix, fibres, and fluid) have constant mass
 224 densities, and no mass exchange processes occur. These assumptions permit
 225 to write the mass balance laws of matrix and fibres as $\dot{\Phi}_{0s} = 0$ and $\dot{\Phi}_{1s} = 0$,
 226 where the material volumetric fractions $\Phi_{0s} = J\phi_{0s}$ and $\Phi_{1s} = J\phi_{1s}$ are the
 227 backward Piola transformations of the spatial volumetric fractions ϕ_{0s} and
 228 ϕ_{1s} , respectively. Clearly, Φ_{0s} and Φ_{1s} are independent of time, but they may
 229 depend on material points. Moreover, in the material formalism, the balance
 230 law of the fluid phase reads

$$\dot{J} + \text{Div } \mathbf{Q} = 0. \quad (7)$$

231 We recall that our formulation assumes that matrix and fibres undergo the
 232 same motion.

233 Hereafter, we consider the limit of negligible inertial forces and the action of
 234 no body forces. Moreover, we assume the validity of Darcy’s law. Consistently
 235 with this assumption, the Cauchy stress tensor of the fluid phase reduces to
 236 $\boldsymbol{\sigma}_f = -\phi_f p \mathbf{g}^{-1}$, where p is called *pore pressure*, and the filtration velocity \mathbf{q}
 237 is expressed as $\mathbf{q} = -\mathbf{k} \text{grad } p$, with \mathbf{k} being the tissue’s permeability tensor.
 238 Analogously, the material filtration velocity is given by $\mathbf{Q} = -\mathbf{K} \text{Grad } p$, where
 239 $\mathbf{K} = J\mathbf{F}^{-1}\mathbf{k}\mathbf{F}^{-T}$ is the material permeability tensor.

240 The employment of Darcy’s law allows to consider only one momentum
 241 balance law for the medium as a whole. By introducing the Cauchy stress
 242 tensor of the solid phase, $\boldsymbol{\sigma}_s = -\phi_s p \mathbf{g}^{-1} + \boldsymbol{\sigma}_{sc}$, where $\boldsymbol{\sigma}_{sc}$ is said to be the
 243 *constitutive part* of $\boldsymbol{\sigma}_s$, and since the system is assumed to be closed with
 244 respect to momentum, the momentum balance law reads $\text{div } \boldsymbol{\sigma} = \mathbf{0}$, where
 245 $\boldsymbol{\sigma} \equiv \boldsymbol{\sigma}_f + \boldsymbol{\sigma}_s$ is the overall Cauchy stress tensor of the medium in the limit
 246 of negligibly small relative velocity $\mathbf{w} = \mathbf{v}_f - \mathbf{v}_s$. To express the balance of
 247 momentum in material formalism, we introduce the first Piola-Kirchhoff stress
 248 tensors of the fluid phase and of the solid phase, i.e., $\mathbf{P}_f = J\boldsymbol{\sigma}_f\mathbf{F}^{-T}$ and
 249 $\mathbf{P}_s = J\boldsymbol{\sigma}_s\mathbf{F}^{-T}$, respectively, and we obtain

$$\text{Div} \left(-Jp\mathbf{g}^{-1}\mathbf{F}^{-T} + \mathbf{P}_{sc} \right) = \mathbf{0}, \quad (8)$$

250 where the term between parentheses is the overall first Piola-Kirchhoff stress
 251 tensor of the system, i.e., the sum of \mathbf{P}_f and \mathbf{P}_s , and $\mathbf{P}_{sc} = J\boldsymbol{\sigma}_{sc}\mathbf{F}^{-T}$ is the
 252 constitutive part of \mathbf{P}_s .

Equations (7) and (8) model the deformation of hydrated soft tissues and the flow of their interstitial fluids, but they cannot describe the dynamics of the internal structure of such tissues. These dynamics, indeed, involve also other processes, which generally occur at different time and length scales, and have distinct biological features. Typical examples of these processes are given by growth, resorption, damage, and reorientation of the network of collagen fibres. A more detailed tissue model should thus consider all these processes and the interactions among them. Nevertheless, we assume here that it is possible to select a modelling range in which one of the aforementioned phenomena can be studied independently of the other ones, at least conceptually [39]. On the basis of this assumption, we propose a theoretical setting in which, besides deformation and fluid flow, we account for the reorientation of fibres in a fibre-reinforced tissue. Moreover, although we present a mathematical model originally conceived for articular cartilage, our results can be extended also to other fibre-reinforced tissues.

We claim that remodelling manifests itself through an evolution in time of the mean angle, Q , which has been introduced in the probability density defined in (5a) and (5b). Thus, we call Q *remodelling variable* from here on. Also ω could be taken as a remodelling variable. However, as done in [39], we prefer here to keep the theory as simple as possible. Thus, we choose ω as a prescribed function of the material points. The remodelling angle Q , instead, evolves starting either from a histological distribution or from a “test” distribution. In the latter case, one aims to see under which conditions the system remodels towards histological patterns. To emphasise that the probability density depends on time through Q (which is now viewed as a function of time and material points), we re-define γ_X and $\bar{\rho}_X$ [cf. (5a) and (5b)] as follows:

$$\bar{\rho}_X(\Theta) = \hat{\rho}(\Theta, X, t) = \frac{\gamma_X(\Theta, X, t)}{2\pi \int_0^{\pi/2} \gamma_X(\Theta', X, t) \sin(\Theta') d\Theta'}, \quad (9a)$$

$$\gamma_X(\Theta) = \hat{\gamma}(\Theta, X, t) = \exp\left(-\frac{[\Theta - Q(X, t)]^2}{2[\omega(X)]^2}\right). \quad (9b)$$

Equations (9a) and (9b) imply that also the probability density Ψ_X depends on time through Q and, consequently, the directional average $\langle\langle \mathfrak{F}_X \rangle\rangle$ must be regarded as a functional of the remodelling variable, Q . To highlight this dependence, we use the notation $\langle\langle \mathfrak{F}_X \rangle\rangle \equiv \langle\langle \mathfrak{F}_X \rangle\rangle(Q)$ from here on.

We remark that the picture of remodelling discussed here and in [22, 39] features some similarities with the framework presented Baaijens et al. [42], of which we were unfortunately unaware at the time we wrote the papers [22, 39]. Thus, we take the occasion of this work to state that a description of remodelling based on the evolution of the mean angle characterising the fibres’ pseudo-Gaussian probability density can also be found in [42] (cf. Equation (20) of [42]). However, the approach proposed in [22], subsequently developed in [39], and further extended in our work, differs from the one presented in [42] due to the different definition of the generalised forces that drive remodelling,

292 and due to the different methodological framework within which the theory of
293 remodelling is established.

294 Following the theory outlined in [19], and subsequently adopted in [27,23],
295 we embrace the line thought according to which the structural evolution of
296 a tissue calls for the introduction of suitable “structural descriptors”. These
297 add themselves to the descriptors associated with the standard kinematics of a
298 tissue, namely the velocities of the solid and the fluid phase (or, alternatively,
299 the velocity of the solid phase, \mathbf{v}_s , and the velocity \mathbf{w} of the fluid relative to
300 the solid). Within the present framework, we identify the tissue’s structural
301 descriptor with the time derivative of the remodelling variable, \dot{Q} , and we call
302 “remodelling forces” the mechanical entities power-conjugate to \dot{Q} [19,27,23].
303 We distinguish these forces into “internal” and “external”, we denote them
304 \mathcal{R}_{int} and \mathcal{R}_{ext} , respectively, and we postulate the force balance [27,22,23]

$$\mathcal{R}_{\text{int}} = \mathcal{R}_{\text{ext}}. \quad (10)$$

305 In conclusion, our theory of remodelling is based on the set of equations
306 (7), (8) and (10), along with (the material counterpart of) Darcy’s law $\mathbf{Q} =$
307 $-\mathbf{K} \text{Grad } p$. We emphasise that we are not regarding Q as an internal variable.
308 Rather, Q is a kinematic variable, having the same “dignity” as the solid phase
309 motion χ , and being determined by solving the balance law (10) associated
310 with it.

311 Remodelling and deformation couple with each other and, together with
312 fluid flow, drive the overall evolution of the tissue. Such evolution is known
313 after the set of equations (7), (8), and (10) is solved, and the motion χ , pressure
314 p , and remodelling variable Q are determined. To this end, the *remodelling*
315 *equation* (10) must be rewritten in such a way that it is explicitly solvable for
316 Q . This, in fact, requires to find admissible constitutive laws for the generalised
317 force \mathcal{R}_{int} . To check for thermodynamic admissibility, we exploit the dissipation
318 inequality.

319 We remark that, since our remodelling variable is a scalar parameter, non-
320 planar remodelling directions cannot be taken into account by our theory. Our
321 choice, however, is meant to keep our model as simple as possible. The model,
322 indeed, can be generalised by introducing two independent remodelling angles,
323 having the meaning of co-latitude and longitude, respectively, and being suf-
324 ficient to determine univocally the unit vector along which the fibres tend to
325 be aligned.

326 **3 Constitutive theory**

327 To close the mathematical model, constitutive laws for \mathbf{K} and \mathbf{P}_{sc} must be
328 supplied. Moreover, whereas the functional form of \mathcal{R}_{ext} has to be prescribed
329 from the outset, \mathcal{R}_{int} must be determined constitutively. In order to do that,
330 a suitable constitutive theory has to be formulated.

3.1 Permeability tensor

Following [43], the permeability tensor of a fibre-reinforced porous medium can be determined by invoking the Representation Theorem for functions valued in the space of symmetric second-order tensors [44, 45]. Here, we consider the results presented in [43] for the case of a medium exhibiting transverse isotropy with respect to \mathbf{M} and, in particular, for the permeability tensor associated with the single fibre, we take the simple expression

$$\mathbf{k}_{\text{fibre}} = k_0 \mathbf{g}^{-1} + J^{-2} k_0 \mathbf{a}, \quad (11)$$

where k_0 is the scalar permeability of the matrix, and \mathbf{a} is defined by

$$\mathbf{a} = \frac{1}{I_4} \mathbf{F} \mathbf{A} \mathbf{F}^T, \quad (12)$$

where $I_4 \equiv I_4(\mathbf{C}, \mathbf{A}) = \mathbf{C} : \mathbf{A}$ is the fourth invariant of \mathbf{C} . Note that the original model of Ateshian and Weiss [43] is expressed in terms of the push-forward $\mathbf{F} \mathbf{A} \mathbf{F}^T$ of the material structure tensor \mathbf{A} , whereas (11) features the normalised spatial structure tensor \mathbf{a} . In (11), we assume for k_0 the Holmes and Mow constitutive law [46]

$$k_0 = \hat{k}_0(J) = k_{0R} \left[\frac{J - \Phi_s}{1 - \Phi_s} \right]^{\kappa_0} \exp\left(\frac{1}{2} m_0 [J^2 - 1]\right), \quad (13)$$

where k_{0R} , κ_0 , and m_0 are model parameters. Note that $\mathbf{k}_{\text{fibre}}$ is a function of \mathbf{F} and \mathbf{A} , i.e., $\mathbf{k}_{\text{fibre}} = \hat{\mathbf{k}}_{\text{fibre}}(\mathbf{F}, \mathbf{A})$. Moreover, the spatial permeability of the tissue, \mathbf{k} , is obtained by computing the directional average of $\mathbf{k}_{\text{fibre}}$, i.e.,

$$\begin{aligned} \mathbf{k} &= \hat{\mathbf{k}}(\mathbf{F}, Q) = \langle\langle \hat{\mathbf{k}}_{\text{fibre}}(\mathbf{F}, \mathbf{A}) \rangle\rangle(Q) \\ &= \hat{k}_0(J) \mathbf{g}^{-1} + J^{-2} \hat{k}_0(J) \mathbf{F} \hat{\mathbf{Z}}(\mathbf{C}, Q) \mathbf{F}^T, \end{aligned} \quad (14)$$

where we introduced the notation

$$\hat{\mathbf{Z}}(\mathbf{C}, Q) = \left\langle\left\langle \frac{\mathbf{A}}{I_4(\mathbf{C}, \mathbf{A})} \right\rangle\right\rangle(Q). \quad (15)$$

Finally, the material permeability $\mathbf{K} = J \mathbf{F}^{-1} \mathbf{k} \mathbf{F}^{-T}$ takes on the form

$$\mathbf{K} = \hat{\mathbf{K}}(\mathbf{C}, Q) = J \hat{k}_0(J) \mathbf{C}^{-1} + J^{-1} \hat{k}_0(J) \hat{\mathbf{Z}}(\mathbf{C}, Q). \quad (16)$$

3.2 Free energy density

Our constitutive theory relies on the assumption that the tissue can be associated with a free energy density consisting of the sum of two contributions, i.e.,

$$W := W_{\text{std}} + W_{\text{rem}}. \quad (17)$$

353 The first summand, W_{std} , is the strain energy density introduced in [16] to
 354 model a transversely isotropic biphasic medium with statistical orientation of
 355 the fibres. The subscript “std” means that it is regarded as *standard* in the
 356 present framework. We write explicitly the expression of W_{std} with the purpose
 357 of highlighting its dependence on the remodelling variable:

$$W_{\text{std}} = \hat{W}_{\text{std}}(\mathbf{C}, Q) = \Phi_s \hat{U}(J(\mathbf{C})) + \Phi_{0s} \hat{W}_0(\mathbf{C}) + \Phi_{1s} \hat{W}_e(\mathbf{C}, Q). \quad (18)$$

358 Here, Φ_{0s} and Φ_{1s} are the volumetric fractions of matrix and fibres in the
 359 reference configuration, respectively, while $\Phi_s = \Phi_{0s} + \Phi_{1s}$ is the volumetric
 360 fraction of the solid phase as a whole in the same configuration. The term
 361 $\hat{U}(J(\mathbf{C}))$ is a penalty enforcing the intrinsic incompressibility of the solid phase
 362 at compaction [16], $\hat{W}_0(\mathbf{C})$ is the isotropic strain energy density of the matrix,
 363 and $\hat{W}_e(\mathbf{C}, Q)$ is referred to as “ensemble potential” [14], and constitutes the
 364 anisotropic contribution to W_{std} , i.e.,

$$\hat{W}_e(\mathbf{C}, Q) = \hat{W}_{1i}(\mathbf{C}) + \langle \hat{W}_{1a}(\mathbf{C}, \mathbf{A}) \rangle(Q). \quad (19)$$

365 The energy densities $\hat{U}(J(\mathbf{C}))$, $\hat{W}_0(\mathbf{C})$, $\hat{W}_{1i}(\mathbf{C})$, and $\hat{W}_{1a}(\mathbf{C}, \mathbf{A})$ are given by

$$\hat{U}(J) = \alpha_0 \mathcal{H}(J_{\text{cr}} - J) [J - J_{\text{cr}}]^{2q} [J - \Phi_s]^{-r}, \quad (20a)$$

$$\hat{W}_0(\mathbf{C}) = \hat{W}_{1i}(\mathbf{C}) = \alpha_0 \frac{\exp(\alpha_1 [I_1 - 3] + \alpha_2 [I_2 - 3])}{[I_3]^{\alpha_3}}, \quad (20b)$$

$$\hat{W}_{1a}(\mathbf{C}, \mathbf{A}) = \mathcal{H}(I_4 - 1) \frac{1}{2} c [I_4 - 1]^2, \quad (20c)$$

366 where \mathcal{H} is the Heaviside function (here, $\mathcal{H}(s) = 0$ for all $s \leq 0$, and $\mathcal{H}(s) =$
 367 1 for all $s > 0$) [38], and we used the short-hand notation $J = J(\mathbf{F}) =$
 368 $\det \mathbf{F}$ for the volume ratio, $I_1 = I_1(\mathbf{C}) = \text{tr}(\mathbf{C})$, $I_2 = I_2(\mathbf{C}) = \frac{1}{2} \{[\text{tr}(\mathbf{C})]^2 -$
 369 $\text{tr}(\mathbf{C}^2)\}$, $I_3 = I_3(\mathbf{C}) = \det \mathbf{C}$ for the three principal invariants of \mathbf{C} , and
 370 $I_4 = I_4(\mathbf{C}, \mathbf{A}) = \mathbf{C} : \mathbf{A}$ for the fourth invariant of \mathbf{C} . In (20a), $J_{\text{cr}} \in]\Phi_s, 1]$
 371 is a “critical” value of J below which the penalty term is switched on to
 372 prevent J from approaching the lower physical bound Φ_s , while $q \geq 2$ and
 373 $r \in]0, 1]$ are model parameters. In (20b) and (20c), α_0 , α_1 , α_2 , α_3 , and c are
 374 model parameters and, in particular, α_0 and c have the same physical units
 375 as the strain energy density and determine the energy scales characterising
 376 the isotropic and anisotropic contributions of \hat{W}_{std} . The term $\hat{W}_{1i}(\mathbf{C})$ is the
 377 isotropic contribution of the fibres to the tissue’s overall strain energy density,
 378 and $\hat{W}_{1a}(\mathbf{C}, \mathbf{A})$ is the anisotropic contribution, which depends on the fibre
 379 alignment through $\mathbf{A} = \mathbf{M} \otimes \mathbf{M}$. The fact that \hat{W}_{1i} is taken here to be
 380 equal to \hat{W}_0 is just a model assumption [38]. We remark that the directional
 381 average of $\hat{W}_{1a}(\mathbf{C}, \mathbf{A})$, i.e., $\langle \hat{W}_{1a}(\mathbf{C}, \mathbf{A}) \rangle$, depends on the remodelling variable,
 382 Q , through the probability density.

383 The idea underlying the definition of the energy density given in (18) can
 384 be found in several works on composite materials [47–49]. In these papers,
 385 a given composite material is modelled within the theory of linear elasticity,
 386 and the elasticity tensor of the material is written as the weighted sum of
 387 the elasticity tensors of its constituents, each multiplied by the corresponding

388 volumetric fraction. In this sum, however, the weights depend on the strain
 389 concentration tensor [49, 50] and, thus, on Eshelby’s fourth-order tensor [51].
 390 In the non-linear framework, instead, the Eshelby-like formulation is not di-
 391 rectly applicable and, if the constituents of a composite material are assumed
 392 to be hyperelastic, the elastic potential of the composite as a whole can be con-
 393 structed by weighing the elastic potentials of the constituents. In some cases,
 394 e.g. [2, 27], the elastic potentials contain the volumetric fractions in their own
 395 definition, whereas we put them in evidence in our formulation. In (18), in-
 396 deed, apart from $\hat{\Phi}_s \hat{U}(J(\mathbf{C}))$, W_{std} is the weighted sum of one contribution
 397 due to the matrix and one due to the fibres, the weights being the volumetric
 398 fractions $\hat{\Phi}_{0s}$ and $\hat{\Phi}_{1s}$.

399 Moreover, in the present work, the isotropic energy densities $\hat{W}_0(\mathbf{C})$ and
 400 $\hat{W}_{1i}(\mathbf{C})$ depend on I_3 , thereby describing a compressible behaviour of the
 401 modelled material, while the anisotropic contribution, $\hat{W}_{1a}(\mathbf{C}, \mathbf{A})$, is assumed
 402 to depend on \mathbf{C} through I_4 only. In fact, the tissue described by (18), (19),
 403 and (20a)–(20c) is compressible and anisotropic, which requires its elastic en-
 404 ergy density to depend both on I_3 and —at least— on I_4 . However, the way
 405 in which compressibility and anisotropy are modelled is not unique and, in
 406 this respect, the additive decomposition of the energy density performed in
 407 (18) and (19), in which the compressible effects are attributed solely to the
 408 isotropic terms, is only one among other possible choices. To give an example,
 409 indeed, in the work by Almeida and Spilker [52] on articular cartilage, the
 410 elastic energy density is anisotropic and compressible, but the decomposition
 411 presented in (18) and (19) was not enforced. We would like to emphasise,
 412 however, that decompositions of this kind are rather customary in the study
 413 of fibre-reinforced hyperelastic materials (see e.g. [2, 27] for the case of blood
 414 vessels). Moreover, strictly speaking, since I_4 can be further decomposed mul-
 415 tiplicatively as $I_4 = I_3^{1/3} \bar{I}_4$, with $\bar{I}_4 = \bar{\mathbf{C}} : \mathbf{A}$ and $\det \bar{\mathbf{C}} = 1$, the anisotropic
 416 part of the energy density still models a compressible material.

417 The second summand of (17), W_{rem} , is the part of the free energy density
 418 that is directly related to remodelling. This term is the main novelty of our
 419 constitutive theory, which is based on the requirement that W_{rem} admits the
 420 representation

$$W_{\text{rem}} = \hat{W}_{\text{rem}}(\mathbf{C}, Q, \text{Grad } Q) = \hat{W}_{\text{str}}(\mathbf{C}, Q) + \hat{W}_{\text{grad}}(\mathbf{C}, \text{Grad } Q). \quad (21)$$

421 The energy densities $\hat{W}_{\text{grad}}(\mathbf{C}, \text{Grad } Q)$ and $\hat{W}_{\text{str}}(\mathbf{C}, Q)$ are given by

$$W_{\text{grad}} = \hat{W}_{\text{grad}}(\mathbf{C}, \text{Grad } Q) = \frac{1}{2} \hat{\mathbf{D}}(\mathbf{C}) : \text{Grad } Q \otimes \text{Grad } Q, \quad (22a)$$

$$W_{\text{str}} = \hat{W}_{\text{str}}(\mathbf{C}, Q) = \hat{\mathcal{A}}(\mathbf{C}) \hat{\mathcal{P}}(Q) \exp(\hat{\alpha}_W(\mathbf{C})Q), \quad (22b)$$

422 where the subscript “grad” indicates that \hat{W}_{grad} depends on the gradient of
 423 the mean angle, while the subscript “str” means that \hat{W}_{str} is directly related
 424 to the internal structure of the tissue. The quantity $\hat{\mathbf{D}}(\mathbf{C})$ is a symmetric,
 425 positive semi-definite, second-order tensor-valued function of \mathbf{C} , $\hat{\mathcal{A}}(\mathbf{C})$ is a
 426 non-negative coefficient with physical units of energy per unit volume, $\hat{\mathcal{P}}(Q)$

427 is a dimensionless, non-negative function of Q , and $\hat{\alpha}_W(\mathbf{C})$ is a dimensionless,
 428 non-negative coefficient. In the absence of deformation, i.e., when \mathbf{C} equals
 429 the material metric tensor \mathbf{G} (which serves here as the “covariant identity
 430 tensor”), we set $\hat{\mathbf{D}}(\mathbf{G}) = \mathbf{D}_0$, $\hat{\mathcal{A}}(\mathbf{C}) = \mathcal{A}_0 \geq 0$, and $\hat{\alpha}_W(\mathbf{G}) = 0$.

431 The term $\hat{W}_{\text{grad}}(\mathbf{C}, \text{Grad } Q)$ is introduced to explicitly account for the
 432 spatial resolution of the remodelling variable, Q . Physically, it represents the
 433 contribution to the overall energy that is set off by the first-order spatial
 434 variations of Q at each material point. To keep the proposed theory at a
 435 minimal level of complexity, we assume that $\hat{W}_{\text{grad}}(\mathbf{C}, \text{Grad } Q)$ is quadratic in
 436 $\text{Grad } Q$. As is the case for other theories based on energy densities that depend
 437 on the gradient of an angular variable (for example, the energy of the Sine-
 438 Gordon model [53]), $\hat{\mathbf{D}}(\mathbf{C})$ could be thought of as a measure of the system’s
 439 “angular stiffness per unit length”. Indeed, it determines the response of the
 440 system to the spatial variations of Q . We remark that, by its own definition,
 441 $\hat{\mathbf{D}}(\mathbf{C})$ is modulated by \mathbf{C} , which means that, in general, the tissue’s angular
 442 stiffness varies with the deformation. If, on the one hand, the evolution of
 443 the remodelling angle Q influences the elastic response of the tissue through
 444 the term $\hat{W}_e(\mathbf{C}, Q)$ [see Equation (18)], the tensor $\hat{\mathbf{D}}(\mathbf{C})$ couples the global
 445 changes of shape of the tissue with its structural transformations, which are
 446 represented by the variations of Q in time and space.

447 Before providing a term-by-term explanation of $\hat{W}_{\text{str}}(\mathbf{C}, Q)$ [see (22b)], we
 448 discuss the logical steps that lead to its functional form. First, we remark that,
 449 since in this work the kinematics of the tissue is described by χ and Q , the
 450 configuration attained by the tissue at time t is determined by both $\chi(X, t)$
 451 and $Q(X, t)$, for all $X \in \mathcal{B}$. Second, we claim that each such configuration
 452 can be associated with an energy that depends on the deformation *and* the
 453 distribution of the fibre mean angle throughout the tissue. Third, by exploiting
 454 the fact that the deformation and the mean angle are independent on each
 455 other, we also claim that there exist distributions of the fibre mean angle that
 456 endow the tissue with non-trivial energies even in the absence of deformation.
 457 Indeed, even though W_{std} reduces to the unessential constant $\hat{W}_{\text{std}}(\mathbf{G}, Q) \equiv$
 458 $\hat{W}_{\text{std}}^{(0)}(Q) = \alpha_0$ in such cases [see (18) and (20a)–(20c)], W_{str} and W_{grad} become

$$\hat{W}_{\text{str}}(\mathbf{G}, Q) \equiv \hat{W}_{\text{str}}^{(0)}(Q) = \mathcal{A}_0 \hat{\mathcal{P}}(Q), \quad (23a)$$

$$\hat{W}_{\text{grad}}(\mathbf{G}, \text{Grad } Q) \equiv \hat{W}_{\text{grad}}^{(0)}(\text{Grad } Q) = \frac{1}{2} \mathbf{D}_0 : \text{Grad } Q \otimes \text{Grad } Q, \quad (23b)$$

459 thereby yielding

$$\begin{aligned} W_{\text{rem}} &\equiv \hat{W}_{\text{rem}}^{(0)}(Q, \text{Grad } Q) = \hat{W}_{\text{str}}^{(0)}(Q) + \hat{W}_{\text{grad}}^{(0)}(\text{Grad } Q), \\ &= \mathcal{A}_0 \hat{\mathcal{P}}(Q) + \frac{1}{2} \mathbf{D}_0 : \text{Grad } Q \otimes \text{Grad } Q, \end{aligned} \quad (24a)$$

$$\begin{aligned} W &\equiv \hat{W}_{\text{std}}^{(0)}(Q) + \hat{W}_{\text{rem}}^{(0)}(Q, \text{Grad } Q) \\ &= \alpha_0 + \hat{W}_{\text{rem}}^{(0)}(Q, \text{Grad } Q). \end{aligned} \quad (24b)$$

460 If \mathbf{D}_0 is positive definite and \mathcal{A}_0 strictly positive, $\hat{W}_{\text{rem}}^{(0)}(Q, \text{Grad } Q)$ is zero
 461 only for those distributions of the fibre mean angle that are spatially uniform

462 and solutions of $\hat{\mathcal{P}}(Q) = 0$. In the jargon of [53], a time-independent field Q
 463 satisfying these conditions is said to be a “*classical vacuum*” configuration for
 464 $\hat{W}_{\text{rem}}^{(0)}(Q, \text{Grad } Q)$, since it determines the lowest energy of the system under
 465 study (zero, in the considered case). In general, however, when Q is not a
 466 vacuum configuration, $\hat{W}_{\text{rem}}^{(0)}(Q, \text{Grad } Q)$ is greater than zero and consists of
 467 the contribution due to the spatial variability of Q , i.e., $\hat{W}_{\text{grad}}^{(0)}(\text{Grad } Q)$, and
 468 of the contribution due to the potential energy density associated with Q , i.e.,
 469 $\hat{W}_{\text{str}}^{(0)}(\text{Grad } Q)$. Thus, up to α_0 , $\hat{W}_{\text{rem}}^{(0)}(Q, \text{Grad } Q)$ is the energy density that
 470 characterises the tissue for a given Q , and the integral

$$\begin{aligned} \mathcal{W}_{\text{rem}}^{(0)}[Q] &= \int_{\mathcal{B}} \hat{W}_{\text{rem}}^{(0)}(Q, \text{Grad } Q) \\ &= \int_{\mathcal{B}} \left\{ \mathcal{A}_0 \hat{\mathcal{P}}(Q) + \frac{1}{2} \mathbf{D}_0 : \text{Grad } Q \otimes \text{Grad } Q \right\} \end{aligned} \quad (25)$$

471 is the tissue’s energy corresponding to Q . In conclusion, and consistently with
 472 what we claimed above, our interpretation of (25) is that any conformation of
 473 the tissue’s internal structure, which is described by selecting an appropriate
 474 distribution of the fibre mean angle, yields an energy. This energy, in turn, is
 475 nonzero as long as the distribution of the fibre mean angle is not a vacuum
 476 configuration.

477 As explained in Section 4.1, we assume that the information on the internal
 478 structure of the tissue is supplied by the histological pattern with which the
 479 fibres are oriented in the undeformed tissue and, thus, by the distribution of
 480 the fibre mean angle associated with it. Such distribution, denoted by Q_{h} ,
 481 can be determined experimentally. In fact, as shown in Fig. 2, it features a
 482 sigmoidal shape and takes on the values $Q_0 = 0$ rad and $Q_1 = \pi/2$ rad at the
 483 lower and upper boundary, respectively, of the cylindrical samples of tissue
 484 adopted in the study [54].

485 Although a functional form for Q_{h} can be obtained by fitting experimental
 486 data [54], we follow here a rather different approach. First, since the sigmoidal
 487 profile of Q_{h} goes from Q_0 to Q_1 , we invoke a formal analogy with the theory of
 488 phase transitions, and we claim that $\hat{W}_{\text{str}}^{(0)}(Q)$ should be a double-well energy
 489 density of the Allen-Cahn type, with $Q_0 = 0$ rad and $Q_1 = \pi/2$ rad being
 490 its global minimum configurations. Thus, with reference to the undeformed
 491 configuration of the tissue, we set

$$\hat{W}_{\text{str}}^{(0)}(Q) \equiv \hat{W}_{\text{AC}}^{(0)}(Q) = \frac{\mathcal{A}_0}{(\pi/4)^4} Q^2 \left(Q - \frac{\pi}{2} \right)^2, \quad (26)$$

492 where $\hat{W}_{\text{AC}}^{(0)}(Q)$ is the Allen-Cahn energy density [26]. We notice that Equations
 493 (23a) and (26) allow to identify $\hat{\mathcal{P}}(Q)$ with

$$\hat{\mathcal{P}}(Q) = \frac{1}{(\pi/4)^4} Q^2 \left(Q - \frac{\pi}{2} \right)^2, \quad (27)$$

494 i.e., with a polynomial of degree four in Q that vanishes for $Q_0 = 0$ rad and
 495 $Q_1 = \pi/2$ rad, and whose global maximum over $[0, \pi/2]$ is attained at $Q_{\max} =$
 496 $\pi/4$ rad.

497 We emphasise that the zeroes of $\hat{\mathcal{P}}(Q)$ are the vacuum configurations of the
 498 Allen-Cahn energy density defined in Equation (26), for which it holds, thus,
 499 $\hat{W}_{\text{AC}}^{(0)}(Q_0) = \hat{W}_{\text{AC}}^{(0)}(Q_1) = 0$. Accordingly, the sigmoidal profile of Q_{h} describes
 500 a transition from Q_0 to Q_1 , and the quantity \mathcal{A}_0 , which is equal to the global
 501 maximum of $\hat{W}_{\text{AC}}^{(0)}(Q)$, defines the height of the energy barrier separating Q_0
 502 from Q_1 .

503 When the deformation is considered, the height of the energy barrier, \mathcal{A}_0 ,
 504 is generally allowed to be modulated by the deformation, and becomes $\hat{\mathcal{A}}(\mathbf{C})$.
 505 Moreover, whereas $\hat{W}_{\text{AC}}^{(0)}(Q)$ is symmetric with respect to $Q = \pi/4$ rad, the
 506 coefficient $\hat{\alpha}_W(\mathbf{C})$ destroys this symmetry for $\mathbf{C} \neq \mathbf{G}$. In conclusion, by using
 507 the expression of $\hat{\mathcal{P}}(Q)$ given in (27), we can interpret the structural part
 508 of the energy density, $\hat{W}_{\text{str}}(\mathbf{C}, Q)$, as a generalised, deformation-dependent
 509 energy density of the Allen-Cahn type, i.e.,

$$\hat{W}_{\text{AC}}(\mathbf{C}, Q) \equiv \hat{W}_{\text{str}}(\mathbf{C}, Q) = \hat{\mathcal{A}}(\mathbf{C})\hat{\mathcal{P}}(Q) \exp(\hat{\alpha}_W(\mathbf{C})Q). \quad (28)$$

510 Although all the results presented in this work have been obtained by
 511 employing $\hat{W}_{\text{AC}}^{(0)}(Q)$ and $\hat{W}_{\text{AC}}(\mathbf{C}, Q)$, these energy densities may have to be
 512 replaced with more appropriate constitutive choices in the case of different
 513 histological distributions of the mean angle, or for tissues other than articular
 514 cartilage. However, if the spatial resolution of the mean angle has to be ex-
 515 plicitly taken into account, a ‘‘gradient-part’’ of the remodelling energy, like
 516 the one defined in (22a), may still be employed.

517 Once the Allen-Cahn energy density (28) is introduced, we claim that Q_{h}
 518 can be determined as the solution of a variational problem. To this end, indeed,
 519 we require that the first-order variation of the functional $\mathcal{W}_{\text{rem}}^{(0)}$, defined in (25),
 520 is zero for arbitrary variations of Q_{h} .

521 In Section 4.1 it will be shown that Q_{h} is computed by solving a differential
 522 equation equipped with the Dirichlet boundary conditions $Q_{\text{h}}(X) = Q_0$, for
 523 all $X \in (\partial\mathcal{B})_{\text{L}}$, and $Q_{\text{h}}(X) = Q_1$, for all $X \in (\partial\mathcal{B})_{\text{U}}$, where $(\partial\mathcal{B})_{\text{L}}$ and $(\partial\mathcal{B})_{\text{U}}$
 524 denote the lower and upper boundaries of \mathcal{B} , respectively. In this case, the
 525 magnitude of \mathbf{D}_0 influences the tendency of the fibre mean angle to become a
 526 straight line connecting Q_0 with Q_1 . This trend, in fact, is obtained in the limit
 527 in which the magnitude of \mathbf{D}_0 goes towards infinity. On the other hand, if the
 528 boundary data are changed in such a way that one of the two Dirichlet condi-
 529 tions is replaced by a homogeneous Neumann condition, then the magnitude
 530 of \mathbf{D}_0 measures the tendency of Q_{h} to distribute itself uniformly throughout
 531 the sample. When this is the case, indeed, the uniformity of Q_{h} increases with
 532 the magnitude of \mathbf{D}_0 . Finally, when the deformation is considered, and the
 533 evolution in time of the fibre mean angle, Q , is studied, $\hat{\mathbf{D}}(\mathbf{C})$ influences the
 534 rate at which Q approaches a stationary solution.

535 3.3 Dissipation Inequality

536 In the present context, the dissipation inequality can be cast in the form [22]
537 (see Appendix B for details)

$$\mathfrak{D} = \mathfrak{D}_I + \mathfrak{D}_{II} + \mathfrak{D}_{III} + \mathfrak{D}_{IV} \geq 0, \quad (29)$$

538 where \mathfrak{D} is the residual dissipation per unit volume of the reference configura-
539 tion, and the summands on the right-hand-side of (29) are given by

$$\begin{aligned} \mathfrak{D}_I = & \left\{ -\mathbf{F} \left(2 \frac{\partial \hat{W}}{\partial \mathbf{C}} \right) + \mathbf{P}_s + \Phi_s p \mathbf{g}^{-1} \mathbf{F}^{-T} \right\} : \mathbf{g} \dot{\mathbf{F}} \\ & + \left\{ \mathbf{P}_f + (J - \Phi_s) p \mathbf{g}^{-1} \mathbf{F}^{-T} \right\} : \mathbf{g} \text{Grad} \mathbf{v}_f, \end{aligned} \quad (30a)$$

$$\mathfrak{D}_{II} = -J \left[\boldsymbol{\pi}_f - p \mathbf{g}^{-1} \text{grad} \phi_f \right] \cdot \mathbf{w}, \quad (30b)$$

$$\mathfrak{D}_{III} = \left\{ - \left[\frac{\partial \hat{W}}{\partial Q} - \text{Div} \left(\frac{\partial \hat{W}}{\partial \text{Grad} Q} \right) \right] + \mathcal{R}_{\text{int}} \right\} \dot{Q}, \quad (30c)$$

$$\mathfrak{D}_{IV} = \text{Div} \left[-T \bar{\boldsymbol{\Omega}}^\eta - \frac{\partial \hat{W}}{\partial \text{Grad} Q} \dot{Q} \right]. \quad (30d)$$

540 Here, $\bar{\boldsymbol{\Omega}}^\eta$ is the entropy flux vector, and \hat{W} is expressed constitutively as

$$\hat{W}(\mathbf{C}, Q, \text{Grad} Q) = \hat{W}_{\text{std}}(\mathbf{C}, Q) + \hat{W}_{\text{rem}}(\mathbf{C}, Q, \text{Grad} Q), \quad (31a)$$

$$\hat{W}_{\text{rem}}(\mathbf{C}, Q, \text{Grad} Q) = \hat{W}_{\text{AC}}(\mathbf{C}, Q) + \frac{1}{2} \hat{\mathbf{D}}(\mathbf{C}) : \text{Grad} Q \otimes \text{Grad} Q. \quad (31b)$$

541 Also the constitutive part of the mechanical stress depends—at least in
542 principle— on the same list of variables. However, to account for the dissipa-
543 tion related to the exchange of momentum between the fluid and the solid
544 phase (which is represented by $\mathfrak{D}_{II} \geq 0$, and leads to Darcy’s law) as well as
545 for the dissipation associated with remodelling (i.e., $\mathfrak{D}_{III} \geq 0$), the complete
546 list of independent constitutive variables is given by \mathbf{F} , Q , $\text{Grad} Q$, \dot{Q} , and
547 \mathbf{w} . Furthermore, we study the dissipation inequality (29) by requiring that
548 \mathfrak{D}_I , \mathfrak{D}_{II} , \mathfrak{D}_{III} , and \mathfrak{D}_{IV} are all non-negative, one independently on the others.
549 Within the present theoretical framework, in which the free energy density
550 \hat{W} features the gradient of the remodelling variable among its arguments, the
551 entropy flux vector does not necessarily reduce to the ratio between a heat
552 flux vector and the absolute temperature [55]. Rather, $\bar{\boldsymbol{\Omega}}^\eta$ is defined by

$$\bar{\boldsymbol{\Omega}}^\eta = -\frac{1}{T} \frac{\partial \hat{W}}{\partial \text{Grad} Q} \dot{Q}, \quad (32)$$

553 thereby establishing that \mathfrak{D}_{IV} vanishes identically. Moreover, since $\dot{\mathbf{F}}$ and
554 $\text{Grad} \mathbf{v}_f$ are not independent constitutive variables, and \mathfrak{D}_I depends linearly
555 on them, the sums between braces in (30a) must be zero to ensure that the

inequality $\mathfrak{D}_I \geq 0$ is fulfilled for arbitrary choices of $\dot{\mathbf{F}}$ and $\text{Grad} \mathbf{v}_f$. Hence, \mathfrak{D}_I vanishes identically. This yields the conditions

$$\mathbf{P}_s = -\phi_s p \mathbf{g}^{-1} \mathbf{F}^{-T} + \mathbf{F} \left(2 \frac{\partial \hat{W}}{\partial \mathbf{C}} \right), \quad (33a)$$

$$\mathbf{P}_f = -(J - \phi_s) p \mathbf{g}^{-1} \mathbf{F}^{-T}, \quad (33b)$$

$$\mathbf{P} = \mathbf{P}_s + \mathbf{P}_f = -J p \mathbf{g}^{-1} \mathbf{F}^{-T} + \mathbf{F} \left(2 \frac{\partial \hat{W}}{\partial \mathbf{C}} \right), \quad (33c)$$

so that the constitutive part \mathbf{P}_{sc} of \mathbf{P}_s and \mathbf{P} is given by

$$\mathbf{P}_{sc} = \mathbf{F} \left(2 \frac{\partial \hat{W}}{\partial \mathbf{C}} \right). \quad (34)$$

Note that, if the free energy density is given as a function of \mathbf{F} , Q , and the spatial gradient of Q , i.e., as $\hat{V}(\mathbf{F}, Q, \text{grad} Q) = \hat{W}(\mathbf{C}, Q, \text{Grad} Q)$, \mathbf{P}_{sc} admits the two equivalent expressions

$$\mathbf{P}_{sc} = \mathbf{F} \left(2 \frac{\partial \hat{W}}{\partial \mathbf{C}} \right) = \mathbf{g}^{-1} \frac{\partial \hat{V}}{\partial \mathbf{F}} + \mathbf{P}_K, \quad (35a)$$

$$\mathbf{P}_K = -\mathbf{g}^{-1} \left(\text{grad} Q \otimes \frac{\partial \hat{V}}{\partial \text{grad} Q} \right) \mathbf{F}^{-T}, \quad (35b)$$

where \mathbf{P}_K is the Piola transform of the Korteweg stress tensor [55]. We emphasise that the presence of \mathbf{P}_K , which is explicit in (35a) and hidden in (34), is a consequence of the fact that our theory employs a free energy density depending on $\text{Grad} Q$.

Finally, we define the dissipative generalised forces $\boldsymbol{\pi}_{fd}$ and \mathcal{N} , i.e.,

$$\boldsymbol{\pi}_{fd} \equiv \boldsymbol{\pi}_f - p \mathbf{g}^{-1} \text{grad} \phi_f, \quad (36a)$$

$$\mathcal{N} \equiv - \left[\frac{\partial \hat{W}}{\partial Q} - \text{Div} \left(\frac{\partial \hat{W}}{\partial \text{Grad} Q} \right) \right] + \mathcal{R}_{int}, \quad (36b)$$

so that the residual dissipation reads

$$\mathfrak{D} = -J \boldsymbol{\pi}_{fd} \cdot \mathbf{w} + \mathcal{N} \dot{Q} \geq 0. \quad (37)$$

While the first term on the right-hand-side of (37) is rather standard and is assumed to lead to Darcy's law in the present framework, the term $\mathcal{N} \dot{Q}$ is "new", in the sense that it is generated by the presence of remodelling [27, 22, 39]. Since the remodelling equation is given by $\mathcal{R}_{int} = \mathcal{R}_{ext}$, and since \mathcal{R}_{int} comprises a dissipative part, \mathcal{N} , as well as a non-dissipative part (which coincides with the terms between brackets in (36b)), we write

$$\mathcal{R}_{int} \equiv \mathcal{N} + \left[\frac{\partial \hat{W}}{\partial Q} - \text{Div} \left(\frac{\partial \hat{W}}{\partial \text{Grad} Q} \right) \right] = \mathcal{R}_{ext}. \quad (38)$$

574 Hence, we obtain

$$\mathcal{N} = - \left[\frac{\partial \hat{W}}{\partial Q} - \text{Div} \left(\frac{\partial \hat{W}}{\partial \text{Grad} Q} \right) \right] + \mathcal{R}_{\text{ext}}. \quad (39)$$

575 Following [22,39], we prescribe \mathcal{N} to be defined through a particular simple
576 constitutive law that is linear in \dot{Q} , i.e.,

$$\mathcal{N} = \hat{\mathcal{N}}(\mathbf{C}, Q, \dot{Q}) = \hat{\Gamma}(\mathbf{C}, Q) \dot{Q}, \quad (40)$$

577 with $\hat{\Gamma}(\mathbf{C}, Q) \geq 0$, so that the remodelling equation becomes

$$\begin{aligned} \hat{\Gamma}(\mathbf{C}, Q) \dot{Q} &= - \left[\frac{\partial \hat{W}}{\partial Q} - \text{Div} \left(\frac{\partial \hat{W}}{\partial \text{Grad} Q} \right) \right] + \mathcal{R}_{\text{ext}} \\ &= - \left[\frac{\partial \hat{W}}{\partial Q} - \text{Div} \left(\hat{\mathbf{D}}(\mathbf{C}) \text{Grad} Q \right) \right] + \mathcal{R}_{\text{ext}}. \end{aligned} \quad (41)$$

578 Equation (41) is the *remodelling equation* that rules the evolution of the re-
579 modelling variable Q . With respect to other pictures of remodelling (for in-
580 stance, those put forward in [27,22,23]), the theory proposed here contains
581 the additional internal remodelling force

$$-\text{Div} \left(\frac{\partial \hat{W}}{\partial \text{Grad} Q} \right) = -\text{Div} \left(\hat{\mathbf{D}}(\mathbf{C}) \text{Grad} Q \right). \quad (42)$$

582 We remark that the terms in brackets in (41) are *not* the functional derivative
583 of \hat{W}_{rem} . Indeed, also \hat{W}_{std} depends on Q and, thus, contributes to the evolution
584 of the remodelling variable. Before going further, we mention that similar
585 constitutive frameworks, based however on the Cahn-Hilliard model, have been
586 proposed in studying tumours in [56–58].

587 3.4 Summary of the model equations and simplifying assumptions

588 The model equations are given by (7), (8), and (41). These have to be solved
589 by providing boundary conditions, as well as initial conditions for χ and Q . In
590 this work, we consider a sample of tissue of cylindrical shape in its reference
591 configuration, \mathcal{B} . We denote by $L = 1$ mm and $R = 1.5$ mm the initial thickness
592 and initial radius of the sample, respectively, and we write the boundary of \mathcal{B}
593 as the disjoint union $\partial \mathcal{B} = (\partial \mathcal{B})_{\text{L}} \sqcup (\partial \mathcal{B})_{\text{U}} \sqcup (\partial \mathcal{B})_{\text{B}}$, where $(\partial \mathcal{B})_{\text{L}}$, $(\partial \mathcal{B})_{\text{U}}$, and
594 $(\partial \mathcal{B})_{\text{B}}$ represent the lower, upper, and lateral portions of $\partial \mathcal{B}$, respectively. The
595 sample is assumed to be transversely isotropic with respect to the direction
596 \mathbf{M}_0 , which coincides with the geometric symmetry axis of the cylinder.

597 The sample is subjected to an unconfined compression test characterised
598 by the boundary conditions (BCs)

$$\text{On } (\partial \mathcal{B})_{\text{U}}, \quad \begin{cases} \chi^3 = \mathbf{g}, \\ (-\mathbf{K} \text{Grad} p) \cdot \mathbf{N} = 0, \end{cases} \quad (43a)$$

$$\text{On } (\partial\mathcal{B})_L, \quad \begin{cases} \chi(X, t) - \chi(X, 0) = \mathbf{0}, \\ (-\mathbf{K}\text{Grad } p) \cdot \mathbf{N} = 0, \end{cases} \quad (43b)$$

$$\text{On } (\partial\mathcal{B})_B, \quad \begin{cases} (-Jp\mathbf{g}^{-1}\mathbf{F}^{-T} + \mathbf{P}_{sc}) \cdot \mathbf{N} = 0, \\ p = 0, \end{cases} \quad (43c)$$

599 where χ^3 is the axial component of the solid phase motion, \mathbf{N} is the field of
600 unit normal to $\partial\mathcal{B}$, and \mathbf{g} is the compressive loading history

$$\mathbf{g}(t) = \begin{cases} L - \frac{t}{T_{\text{ramp}}}u_T, & \text{for } t \in [0, T_{\text{ramp}}], \\ L - u_T, & \text{for } t \in]T_{\text{ramp}}, T_{\text{end}}]. \end{cases} \quad (44)$$

601 The target displacement $u_T = 0.2$ mm is reached by $(\partial\mathcal{B})_U$ at $T_{\text{ramp}} = 20$ s,
602 and then maintained up to $T_{\text{end}} = 100$ s. The BCs (43a) and (43b) indicate
603 that $(\partial\mathcal{B})_U$ and $(\partial\mathcal{B})_L$ are impermeable, with $(\partial\mathcal{B})_U$ being displaced axially
604 according to \mathbf{g} , and $(\partial\mathcal{B})_L$ being kept fixed. The BCs (43c), instead, imply that
605 $(\partial\mathcal{B})_B$ is permeable and free of applied surface forces. A schematic description
606 of the considered benchmark test is given in Fig. 1.

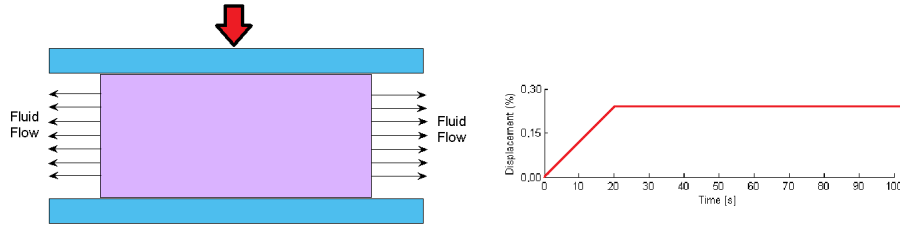


Fig. 1 Schematic description of the considered loading history. The sample is compressed along the axial direction by means of a loading ramp up to $t \leq T_{\text{ramp}} = 20$ s, and the load is then maintained up to $T_{\text{end}} = 100$ s.

607 In addition to (43a)–(43c), we also prescribe the BCs for the remodelling
608 variable, Q , i.e.,

$$\text{On } (\partial\mathcal{B})_U, \quad Q(X, t) = \frac{\pi}{2} \text{ rad}, \quad \forall t \in]0, T_{\text{end}}], \quad (45a)$$

$$\text{On } (\partial\mathcal{B})_L, \quad Q(X, t) = 0 \text{ rad}, \quad \forall t \in]0, T_{\text{end}}], \quad (45b)$$

$$\text{On } (\partial\mathcal{B})_B, \quad (-\hat{\mathbf{D}}(\mathbf{C})\text{Grad } Q) \cdot \mathbf{N} = 0, \quad \forall t \in]0, T_{\text{end}}] \quad (45c)$$

609 Finally, the initial condition on χ is expressed by requiring that the reference
610 configuration, which coincides here with the initial one, is undeformed, while
611 the initial condition on Q can be either obtained by fitting experimental data
612 or computed via preliminary calculations, as explained in Section 4.1.

613 We remark that the boundary conditions imposed on Q are necessary to
614 solve the partial differential equation governing its spatiotemporal evolution.
615 Among various possible choices (i.e., boundary conditions of Dirichlet, Neu-
616 mann, or mixed type), we chose Dirichlet boundary conditions because they

617 are easier to handle from a numerical point of view, and because they are
 618 consistent with the histological information on the pattern of fibre alignment
 619 within the tissue. Clearly, imposing these conditions on the upper and lower
 620 boundary of the sample prescribes the values of the remodelling variable on
 621 these surfaces. This, in turn, amounts to restrict the remodelling process only
 622 to the internal points of the sample, and, in the case studied in Section 4.1,
 623 guides the distribution of the fibre mean angle towards the expected result.
 624 However, this requirement seems to us weaker, and therefore more general,
 625 than prescribing the histological profile *a priori*, or selecting an *ad hoc* remod-
 626 elling force \mathcal{R}_{ext} . Moreover, the use of boundary conditions of different type,
 627 and their impact on the solution describing the distribution of the fibre mean
 628 angle is part of our current investigations.

629 Before going further, it is important to analyse the explicit expression
 630 of $2(\partial\hat{W}/\partial\mathbf{C})$ and $\partial\hat{W}/\partial Q$. For this purpose, we invoke the constitutive laws
 631 (18)–(26), (31a) and (31b), and we enforce the simplifying assumptions $\hat{\mathcal{A}}(\mathbf{C}) =$
 632 \mathcal{A}_0 , $\hat{\mathbf{D}}(\mathbf{C}) = D_0\mathbf{G}^{-1}$ (the inverse metric \mathbf{G}^{-1} here serves as the “contravariant
 633 identity tensor”), and $\hat{\Gamma}(\mathbf{C}, Q) = \Gamma$, where \mathcal{A}_0 , D_0 , and Γ are assumed to be
 634 constant. Moreover, we set

$$\hat{\alpha}_W(\mathbf{C}) = \frac{1}{2}a[I_1(\bar{\mathbf{C}}) - 3]^2, \quad (46)$$

635 with a being a non-negative scalar constant, and $\bar{\mathbf{C}} = J^{-2/3}\mathbf{C}$. We need to
 636 clarify, however, that, since D_0 and \mathcal{A}_0 must vanish in the absence of fibres,
 637 both D_0 and \mathcal{A}_0 should be expressed by means of continuous functions of the
 638 volumetric fraction of the fibres, Φ_{1s} , that tend to zero when Φ_{1s} tends to zero.
 639 Furthermore, since Φ_{1s} is a function of the material point, D_0 and \mathcal{A}_0 should
 640 depend on the material point too. Therefore, the assumption of constant D_0
 641 and \mathcal{A}_0 means that these coefficients correspond to averaged values of Φ_{1s} . In
 642 the cases in which this hypothesis is invalid, D_0 and \mathcal{A}_0 should be reformulated
 643 as $D_0 = \Phi_{1s}\tilde{D}_0$ and $\mathcal{A}_0 = \Phi_{1s}\tilde{\mathcal{A}}_0$, where $\tilde{D}_0 \geq 0$ and $\tilde{\mathcal{A}}_0 \geq 0$ may also depend
 644 on the material point, in general.

645 The assumptions done so far imply that the free energy density used for
 646 simulations is given by

$$\hat{W}(\mathbf{C}, Q, \text{Grad}Q) = \hat{W}_{\text{std}}(\mathbf{C}, Q) + \hat{W}_{\text{rem}}(\mathbf{C}, Q, \text{Grad}Q), \quad (47a)$$

$$\hat{W}_{\text{rem}}(\mathbf{C}, Q, \text{Grad}Q) = \hat{W}_{\text{AC}}(\mathbf{C}, Q) + \frac{1}{2}D_0\|\text{Grad}Q\|^2, \quad (47b)$$

$$\hat{W}_{\text{AC}}(\mathbf{C}, Q) = \mathcal{A}_0\hat{\mathcal{P}}(Q)\exp(\hat{\alpha}_W(\mathbf{C})Q), \quad (47c)$$

647 with $\hat{\alpha}_W(\mathbf{C})$ being defined in (46). Hence, we find

$$\begin{aligned} \hat{\mathbf{P}}_{\text{sc}} &= \mathbf{F} \left(2 \frac{\partial\hat{W}}{\partial\mathbf{C}} \right) = \mathbf{F} \left(2 \frac{\partial\hat{W}_{\text{std}}}{\partial\mathbf{C}} \right) + \mathbf{F} \left(2 \frac{\partial\hat{W}_{\text{AC}}}{\partial\mathbf{C}} \right) \\ &= \mathbf{F} \left(2 \frac{\partial\hat{W}_{\text{std}}}{\partial\mathbf{C}} \right) + \hat{W}_{\text{AC}}Q\mathbf{F} \left(2 \frac{\partial\hat{\alpha}_W}{\partial\mathbf{C}} \right) \end{aligned}$$

$$= \mathbf{F} \left(2 \frac{\partial \hat{W}_{\text{std}}}{\partial \mathbf{C}} \right) + 2 \hat{W}_{\text{AC}}(\mathbf{C}, Q) Q a [I_1(\bar{\mathbf{C}}) - 3] J^{-2/3} \mathbf{F} \text{Dev}^* \mathbf{G}^{-1}, \quad (48a)$$

$$\begin{aligned} \frac{\partial \hat{W}}{\partial Q} &= \frac{\partial \hat{W}_{\text{std}}}{\partial Q} + \frac{\partial \hat{W}_{\text{rem}}}{\partial Q} = \frac{\partial \hat{W}_{\text{std}}}{\partial Q} + \frac{\partial \hat{W}_{\text{AC}}}{\partial Q} \\ &= \frac{\partial \hat{W}_{\text{std}}}{\partial Q} + \mathcal{A}_0 \frac{\partial \hat{\mathcal{P}}}{\partial Q} e^{\hat{\alpha}_W Q} + \mathcal{A}_0 \hat{\mathcal{P}} e^{\hat{\alpha}_W Q} \hat{\alpha}_W, \end{aligned} \quad (48b)$$

648 where $\text{Dev}^* \mathbf{G}^{-1} := \mathbf{G}^{-1} - \frac{1}{3}(\mathbf{G}^{-1} : \mathbf{C}) \mathbf{C}^{-1}$ is the deviatoric part of \mathbf{G}^{-1} with
649 respect to the deformed metric tensor \mathbf{C} . In particular, it holds that

$$\begin{aligned} \frac{\partial \hat{W}_{\text{std}}}{\partial Q} &= \frac{\Phi_{1s}}{\omega^2} \text{cov} \left(\Theta, \hat{W}_{1a}(\mathbf{C}, \hat{\mathbf{A}}(\Theta, \Phi)) \right) \\ &= \Phi_{1s} \frac{\langle\langle \Theta \hat{W}_{1a}(\mathbf{C}, \hat{\mathbf{A}}(\Theta, \Phi)) \rangle\rangle - \langle\langle \Theta \rangle\rangle \langle\langle \hat{W}_{1a}(\mathbf{C}, \hat{\mathbf{A}}(\Theta, \Phi)) \rangle\rangle}{\omega^2}, \end{aligned} \quad (49a)$$

$$\frac{\partial \hat{\mathcal{P}}}{\partial Q} = \frac{4}{(\pi/4)^4} Q \left(Q - \frac{\pi}{2} \right) \left(Q - \frac{\pi}{4} \right), \quad (49b)$$

650 where the notation $\mathbf{A} = \hat{\mathbf{A}}(\Theta, \Phi)$ means that the structure tensor has to be
651 rewritten as a function of the angular coordinates Θ and Φ . The right-hand-
652 side of (49a) is the covariance between Θ and $\hat{W}_{1a}(\mathbf{C}, \hat{\mathbf{A}}(\Theta, \Phi))$ and, since it
653 involves the computation of directional averages, it has to be understood as a
654 function of Q . In summary, the model equations are given by

$$\text{Div} \left[-J p \mathbf{g}^{-1} \mathbf{F}^{-\text{T}} + \mathbf{F} \left(2 \frac{\partial \hat{W}}{\partial \mathbf{C}} \right) \right] = \mathbf{0}, \quad (50a)$$

$$\dot{J} = \text{Div} (\mathbf{K} \text{Grad} p), \quad (50b)$$

$$\Gamma \dot{Q} = - \left[\frac{\partial \hat{W}}{\partial Q} - \text{Div} (D_0 \mathbf{G}^{-1} \text{Grad} Q) \right] + \mathcal{R}_{\text{ext}}, \quad (50c)$$

655 where the constitutive results reported in (48a)–(49b) have to be used. For
656 the numerical computations we use the assumption that the model parameters
657 depend only on the axial normalised coordinate $\xi = X^3/L \in [0, 1]$, with X^3
658 being the axial coordinate of the point $X \in \mathcal{B}$. In particular, the volumetric
659 fractions Φ_{0s} , Φ_{1s} , and Φ_s are given by

$$\Phi_{0s} \equiv \Phi_{0s}(\xi) = -0.062 \xi^2 + 0.038 \xi + 0.046, \quad (51a)$$

$$\Phi_{1s} \equiv \Phi_{1s}(\xi) = +0.062 \xi^2 - 0.138 \xi + 0.204, \quad (51b)$$

$$\Phi_s \equiv \Phi_s(\xi) = -0.100 \xi + 0.250. \quad (51c)$$

660 We also introduce the void ratio $e_R(\xi) = (1 - \Phi_s(\xi))/\Phi_s(\xi)$, which is completely
661 defined by (51c). Then, we prescribe the reference scalar permeability k_{0R} used

662 in (13) to be [59,38]

$$k_{0R} \equiv k_{0R}(\xi) = k_{0R}^{(0)} \left[\frac{e_R(\xi)}{e_R^{(0)}} \right]^{\kappa_0} \exp \left(\frac{1}{2} m_0 \left[\left(\frac{1 + e_R(\xi)}{1 + e_R^{(0)}} \right)^2 - 1 \right] \right), \quad (52)$$

663 with $k_{0R}^{(0)} = 0.003 \text{ mm}^4 \text{ N}^{-1} \text{ s}^{-1}$, $\kappa_0 = 0.0848$, $m_0 = 4.638$ [46], and $e_R^{(0)} = 4.0$
 664 [60]. For the “standard” part of the free energy density, \hat{W}_{std} , we adopt the
 665 parameters $\alpha_0 = 0.1250 \text{ MPa}$, $\alpha_1 = 0.7778$, $\alpha_2 = 0.1111$, and $c = 7.5 \text{ MPa}$
 666 [61] for \hat{W}_0 , \hat{W}_{1i} , and \hat{W}_{1a} (see [38] and the reference therein), and $q = 2$,
 667 $r = 1/2$, and $J_{\text{cr}}(\xi) = \Phi_s(\xi) + 0.1$ for the penalty term \hat{U} . For the remodelling
 668 part, \hat{W}_{rem} , we use several pairs of D_0 and \mathcal{A}_0 (an example of such values is
 669 $D_0 = 1.0 \cdot 10^{-4} \text{ N/rad}$ and $\mathcal{A}_0 = 154 \text{ Pa}$) and we let a take the values $a = 0$
 670 or $a = 10^3$ (clearly, also other values may be chosen). Finally, although in a
 671 previous paper [54] we took the function

$$\omega(\xi) = 10^3 [(1 - \xi)\xi]^4 + 0.03 \quad (53)$$

672 to compute the variance $[\omega(\xi)]^2$, in the simulations performed for this work,
 673 we set $\omega(\xi) = \omega_0 = 0.3$ for all $\xi \in [0, 1]$.

674 4 The remodelling equation

675 In this section, we study two limit cases of the remodelling equation. The first
 676 case shows that a stationary solution of the remodelling equation recovers the
 677 profile taken from [54], which mimics the histological pattern of fibre orienta-
 678 tion. In the second case, we search for those stationary solutions to (50c)
 679 that may represent admissible target profiles of the remodelling variable. The
 680 existence of these solutions depends on the choice of the boundary conditions.

681 4.1 The histological profile

682 As anticipated in Section 3.2, the reason for choosing the functional forms (21)–
 683 (27) is histological. To see this, let us assume that the reference, undeformed
 684 configuration of the sample coincides with the region of space that it occupies
 685 at time $t = 0$. In this configuration, the pattern of the fibre orientation can
 686 be observed experimentally, and an expression of the mean angle fitting the
 687 histological data is given by [54]

$$Q_{\text{fit}}(\xi) = \frac{\pi}{2} \left\{ 1 - \cos \left(\frac{\pi}{2} \left[-\frac{2}{3}\xi^2 + \frac{5}{3}\xi \right] \right) \right\}, \quad (54)$$

688 where ξ is the normalised axial coordinate. The coordinate ξ is zero at the
 689 bone-cartilage interface (also known as “tidemark”), which coincides with the
 690 sample’s lower boundary $(\partial\mathcal{B})_L$, and is equal to unity at the articular surface,
 691 represented by the upper boundary $(\partial\mathcal{B})_U$. Note that, in this configuration,

692 the fluid is assumed to be at rest and the pore pressure is taken equal to zero
 693 everywhere in the tissue. The function Q_{fit} takes the values $Q_{\text{fit}}(0) = 0$ rad
 694 and $Q_{\text{fit}}(1) = \pi/2$ rad, thereby meaning that the fibres are almost perfectly
 695 parallel to the specimen's symmetry axis at the tidemark, and almost perfectly
 696 orthogonal to it at the articular surface. Thus, by construction, Q_{fit} mimics
 697 the histological profile of the fibre mean angle.

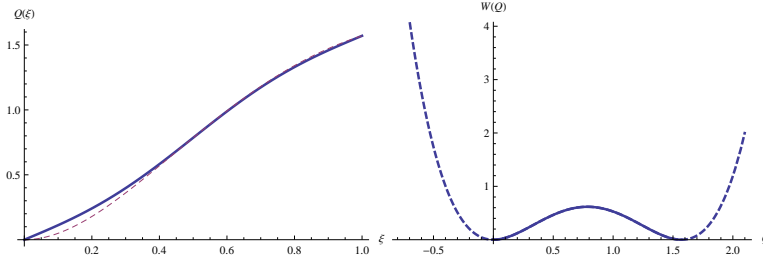


Fig. 2 (a): Comparison between $Q_{\text{fit}}(\xi)$ and $Q(\xi)$ for a given set of parameters A_0 , D_0 , and specimen height L . For the chosen parameters, the two curves deviate appreciably from each other only for values of ξ close to zero, i.e., in the deep zone of articular cartilage. (b): The Allen-Cahn free energy density in (26) is represented. The dashed parts lie outside of the considered range $[0, \pi/2]$. In fact, the two minima correspond to $Q(0) = 0$ rad and $Q(1) = \pi/2$ rad, respectively.

698 We take inspiration from the aforementioned experimental observations
 699 to claim that the angles $Q_{\text{fit}}(0) = 0$ rad and $Q_{\text{fit}}(1) = \pi/2$ rad are “critical”
 700 values of the fibre mean angle and, more importantly, that the histological
 701 profile is the result of a “structural phase transition” occurring in articular
 702 cartilage at some stage of its formation (thus, *prior* to any mechanical test
 703 performed on the tissue either *in vitro* or *in silico*). In our view, this phase
 704 transition consists of a structural reorganisation of the tissue, and leads to
 705 the histological fibre distribution observed in the undeformed configuration.
 706 To see whether our interpretation is compatible with experimental evidence,
 707 we endow the tissue with a free energy density of the Allen-Cahn type, which
 708 we assume to exist independently of deformation, and we suggest that the
 709 histological profile is the solution of a variational problem formulated in the
 710 undeformed configuration. In fact, we choose $\hat{W}_{\text{rem}}^{(0)}(Q, \text{Grad } Q)$ as specified
 711 in (24a), with $\hat{W}_{\text{str}}^{(0)}(Q) = \hat{W}_{\text{AC}}^{(0)}(Q)$ as in (26), and we require the functional
 712 derivative of $\mathcal{W}_{\text{rem}}^{(0)}$ [see Eq. (25)] to be zero. This amounts to solving the partial
 713 differential equation

$$\frac{\partial \hat{W}_{\text{rem}}^{(0)}}{\partial Q} - \text{Div} \left[\frac{\partial \hat{W}_{\text{rem}}^{(0)}}{\partial \text{Grad } Q} \right] = 0 \quad \Rightarrow \quad (55a)$$

$$\frac{\partial \hat{W}_{\text{AC}}^{(0)}}{\partial Q} - \text{Div} [D_0 \mathbf{G}^{-1} \text{Grad } Q] = 0 \quad \Rightarrow \quad (55b)$$

$$\frac{4\mathcal{A}_0}{(\pi/4)^4}Q\left(Q - \frac{\pi}{2}\right)\left(Q - \frac{\pi}{4}\right) - \text{Div}[D_0\mathbf{G}^{-1}\text{Grad}Q] = 0. \quad (55c)$$

714 Let us now focus on a particularly simple case in which the sample is a
 715 cylinder (as specified in section 3.4), and Q depends only on the normalised
 716 axial coordinate ξ . The coefficient D_0 is set equal to zero from the outset when
 717 the spatial resolution of the remodelling variable is not explicitly taken into
 718 account, and is greater than zero otherwise. According to these hypotheses,
 719 when $D_0 \neq 0$, (55c) becomes

$$\frac{4\mathcal{A}_0L^2}{(\pi/4)^4D_0}Q\left(Q - \frac{\pi}{2}\right)\left(Q - \frac{\pi}{4}\right) - \frac{d^2Q}{d\xi^2} = 0, \quad (56)$$

720 with the boundary conditions $Q(0) = 0$ rad and $Q(1) = \pi/2$ rad. Comparing
 721 the solution of (56), $Q_h(\xi)$, with the function $Q_{\text{fit}}(\xi)$ assigned in (54) allows
 722 to estimate the combination of parameters \mathcal{A}_0 and D_0 that minimises the
 723 distance between $Q_h(\xi)$ and $Q_{\text{fit}}(\xi)$ (see Fig. 2). This result seems to suggest
 724 that, after the model parameters are calibrated on the basis of experimental
 725 observations, and the histologically based boundary conditions $Q(0) = 0$ rad
 726 and $Q(1) = \pi/2$ rad are enforced, the functional form of the histological profile
 727 need not be prescribed by fitting experimental data, since it may be computed
 728 as the extremum of the remodelling energy (25).

729 As anticipated in Section 3.4, the Dirichlet boundary conditions imposed
 730 on the values taken by Q at the lower and upper boundary of the sample
 731 enhance the convergence of the solution towards Q_{fit} . This behaviour, however,
 732 manifests itself only at $(\partial\mathcal{B})_L$ and $(\partial\mathcal{B})_U$, where the conditions (45a) and
 733 (45b) comply with the minimum configurations of $\hat{W}_{AC}^{(0)}(Q)$. In general, instead,
 734 when the evolution of the fibre mean angle is studied in conjunction with the
 735 deformation of the tissue, our model can produce a profile that is far from
 736 the histological one (see e.g. Fig. (8)). Moreover, other boundary conditions,
 737 which may depend on time, deformation, or stress, could also be considered
 738 to better describe other physical occurrences.

739 We remark that the profile reported in Fig. 2(a) has been obtained for
 740 $L = 1$ mm and the ratio $(\mathcal{A}_0L^2)/D_0 = 1.54$. A pair of model parameters
 741 \mathcal{A}_0 and D_0 complying with this ratio is given by $D_0 = 1.0 \cdot 10^{-4}$ N/rad and
 742 $\mathcal{A}_0 = 154$ Pa.

743 4.2 “Target fields” and stationary solutions

744 An essential issue in the mechanical theories of remodelling is the identification
 745 of the generalised forces that drive the structural evolution of the considered
 746 system. Before studying this problem within our theoretical framework, we
 747 review the case in which the free energy density does not feature terms of the
 748 type $\hat{W}_{\text{rem}}(\mathbf{C}, Q, \text{Grad}Q)$. In such a setting, the remodelling law (50c) reduces
 749 to the ordinary differential equation

$$\Gamma\dot{Q} = \mathcal{R}_{\text{ext}} - \frac{\partial\hat{W}_{\text{std}}}{\partial Q}(\mathbf{C}, Q), \quad (57)$$

750 and the evolution of Q is entirely driven by the difference between \mathcal{R}_{ext} and
 751 $\partial\hat{W}_{\text{std}}/\partial Q$. More specifically, while $\partial\hat{W}_{\text{std}}/\partial Q$ is dictated by the choice of \hat{W}_{std} ,
 752 \mathcal{R}_{ext} characterises the coupling between Q and the other mechanical variables
 753 of the system. For example, following Hariton et al. [62], \mathcal{R}_{ext} may be related
 754 to stress by claiming that the direction along which the fibres tend to align
 755 themselves is driven by the eigenvalues of Cauchy stress tensor. To account
 756 for this requirement, it is possible to prescribe \mathcal{R}_{ext} as [27]

$$\mathcal{R}_{\text{ext}} \equiv \frac{\partial\hat{W}_{\text{std}}}{\partial Q}(\mathbf{C}, Q_{\text{T}}), \quad (58)$$

757 where Q_{T} is a suitably constructed *target angle*, i.e., a “privileged” distribution
 758 of the mean angle entirely determined by stress. We emphasise that, since the
 759 principal stresses are time-dependent, the target angle varies in time [27].
 760 Thus, \dot{Q} is generally non-zero until Q is not equal to Q_{T} . If, however, (57) and
 761 (58) are studied in the limit in which Q_{T} tends to some stationary distribution
 762 Q_{T}^{∞} , the remodelling process ceases asymptotically when Q approaches one of
 763 the stationary solutions of the evolution equation

$$\Gamma\dot{Q} = \frac{\partial\hat{W}_{\text{std}}}{\partial Q}(\mathbf{C}, Q_{\text{T}}^{\infty}) - \frac{\partial\hat{W}_{\text{std}}}{\partial Q}(\mathbf{C}, Q). \quad (59)$$

764 In particular, if the dependence of \hat{W}_{std} on Q implies the uniqueness of the
 765 stationary solution to (59), then $Q_{\text{st}} \equiv Q_{\text{T}}^{\infty}$ is the stationary mean angle
 766 towards which the system remodels.

767 We remark that the existence of solutions of the type $Q_{\text{st}} = Q_{\text{T}}^{\infty}$ is closely
 768 related to the introduction of the target angle and the external remodelling
 769 force, \mathcal{R}_{ext} . In a previous work [39], however, we searched for stationary so-
 770 lutions to (57) in the limit case of vanishing, or negligibly small, \mathcal{R}_{ext} and
 771 with \hat{W}_{std} defined as in (18)–(20c). Consequently, we solved the remodelling
 772 equation

$$\Gamma\dot{Q} = -\frac{\partial\hat{W}_{\text{std}}}{\partial Q}, \quad (60)$$

773 and we found that \dot{Q} tended asymptotically towards zero because the condition

$$0 = -\frac{\partial\hat{W}_{\text{std}}}{\partial Q} = -\frac{\Phi_{1s}}{\omega^2} \text{cov}(\Theta, \hat{W}_{1a}(\mathbf{C}, \hat{\mathbf{A}}(\Theta, \Phi))) \quad (61)$$

774 applied for large values of t . This result was respected because the deformation
 775 obtained for large values of t implied the asymptotic fulfilment of the inequality
 776 $I_4 \leq 1$, even though (61) admitted no roots in the variable Q . We remark *a*
 777 *posteriori* that, if \mathcal{R}_{ext} had been considered in [39] in the form given in (58),
 778 the presence of the Heaviside function $\mathcal{H}(I_4 - 1)$ in the definition of \hat{W}_{std} would
 779 have made it tend asymptotically towards zero for the deformations attained
 780 in the tissue for large times.

781 The theoretical setting developed in this work is conceived to improve
 782 the results obtained in [39]. To this end, it proposes to describe remodelling
 783 through (50c), which introduces two novelties: It accounts for the spatial res-
 784 olution of the fibre mean angle, and it defines the remodelling part of the sys-
 785 tem’s free energy density, \hat{W}_{rem} , where $\exp(\hat{\alpha}_W(\mathbf{C})Q)$ describes a non-trivial
 786 coupling between Q and the deformation [see (31b) and (28)]. By enforcing
 787 the simplifying assumptions done in Section 3.4, and neglecting \mathcal{R}_{ext} from the
 788 outset, the remodelling equation (50c) becomes

$$\Gamma\dot{Q} = \text{Div} [D_0\mathbf{G}^{-1}\text{Grad}Q] - \frac{\partial\hat{W}_{\text{AC}}}{\partial Q} - \frac{\partial\hat{W}_{\text{std}}}{\partial Q}. \quad (62)$$

789 Note that, similarly to \mathcal{R}_{ext} in (57), also the term $-\partial\hat{W}_{\text{AC}}/\partial Q$ plays a “driving”
 790 role in the evolution of the fibre mean angle and, in fact, we switch off \mathcal{R}_{ext} with
 791 the purpose of focussing on the implications of $-\partial\hat{W}_{\text{AC}}/\partial Q$ on remodelling.
 792 In this case, since no stress-driven target angle is considered *a priori* in the
 793 model, $-\partial\hat{W}_{\text{AC}}/\partial Q$ modulates the evolution of Q through the deformation.
 794 In this framework, however, a “target angle” is—if it exists—a stationary
 795 solution to (62), i.e., a function obtained by solving

$$-\left[\frac{\partial\hat{W}_{\text{std}}}{\partial Q} + \frac{\partial\hat{W}_{\text{AC}}}{\partial Q} - \text{Div} (D_0\mathbf{G}^{-1}\text{Grad}Q) \right] = 0, \quad (63)$$

796 together with (50a), (50b), and the boundary conditions prescribed in Section
 797 3.4. For example, in the case of articular cartilage, we impose $Q(X) = 0$ rad
 798 for $X \in (\partial\mathcal{B})_{\text{L}}$ and $Q(X) = \pi/2$ rad for $X \in (\partial\mathcal{B})_{\text{U}}$, thereby requiring the
 799 congruence of Q with the initial histological data for all the points of the
 800 lower boundary, $(\partial\mathcal{B})_{\text{L}}$, and for all the points of the upper boundary, $(\partial\mathcal{B})_{\text{U}}$,
 801 of the cartilage specimen taken for benchmarking (note that the dependence
 802 of Q on time has been suppressed here, because we are looking for stationary
 803 solutions). We notice that, notwithstanding their similar form, (63) is quite
 804 different from (55c). The differences are essentially due to two facts. Firstly, in
 805 (63), both the contribution to remodelling stemming from the standard strain
 806 energy density, \hat{W}_{std} , and the Allen-Cahn contribution, \hat{W}_{AC} , are accounted
 807 for. Secondly, in (63), \hat{W}_{AC} takes into account the coupling between deforma-
 808 tion and remodelling, since it depends both on \mathbf{C} and on Q . In particular, the
 809 introduction of the factor $\exp(\hat{\alpha}_W(\mathbf{C})Q)$ shifts, for a given \mathbf{C} , the maximum
 810 configuration of $\hat{W}_{\text{AC}}(\mathbf{C}, Q)$ from $\pi/4$ to the deformation dependent value

$$Q_{\text{max}} \equiv Q_{\text{max}}(\mathbf{C}) = \frac{-8 + \pi\hat{\alpha}_W(\mathbf{C}) + \sqrt{64 + \pi^2[\hat{\alpha}_W(\mathbf{C})]^2}}{4\hat{\alpha}_W(\mathbf{C})}, \quad (64)$$

811 for $\hat{\alpha}_W(\mathbf{C}) \neq 0$. In the limit of vanishing $\hat{\alpha}_W(\mathbf{C})$, the value $Q_{\text{max}} = \pi/4$ rad
 812 is recovered.

813 In the following, we speak of “*standard remodelling*” when we refer to (60),
 814 and we call “*non-standard remodelling*” the process described by (62).

5 Numerical Tests

In this section, we report the results of the Finite Element implementation of the unconfined compression test described in Section 3.4. To this end, we consider the weak form of the model equations (50a)–(50c) associated with the BCs (43a)–(43c) and (45a)–(45c), i.e.,

$$\mathcal{F}(\chi, p, Q) = \mathcal{F}_\chi(\chi, p, Q) + \mathcal{F}_p(\chi, p, Q) + \mathcal{F}_Q(\chi, Q) = 0, \quad (65)$$

where the functionals \mathcal{F}_χ , \mathcal{F}_p , and \mathcal{F}_Q are defined as

$$\mathcal{F}_\chi(\chi, p, Q) = \int_{\mathcal{B}} \left[-Jp \mathbf{g}^{-1} \mathbf{F}^{-T} + \hat{\mathbf{P}}_{\text{sc}}(\mathbf{F}, Q) \right] : \mathbf{g} \text{Grad } \tilde{\mathbf{u}}, \quad (66a)$$

$$\mathcal{F}_p(\chi, p, Q) = \int_{\mathcal{B}} \left[J\tilde{p} + (\text{Grad } \tilde{p}) \hat{\mathbf{K}}(\mathbf{C}, Q)(\text{Grad } p) \right], \quad (66b)$$

$$\begin{aligned} \mathcal{F}_Q(\chi, Q) &= \int_{\mathcal{B}} [D_0 \mathbf{G}^{-1} \text{Grad } Q] \text{Grad } \tilde{\Omega} \\ &+ \int_{\mathcal{B}} \left[\Gamma \dot{Q} + \frac{\partial \hat{W}_{\text{std}}}{\partial Q}(\mathbf{C}, Q) + \frac{\partial \hat{W}_{\text{AC}}}{\partial Q}(\mathbf{C}, Q) \right] \tilde{\Omega}. \end{aligned} \quad (66c)$$

Here, $\tilde{\mathbf{u}}$ and $\tilde{\Omega}$ are the test velocities associated with the solid phase motion, χ , and the mean angle, Q , respectively, and \tilde{p} is the test pressure.

Equations (66a)–(66c) are discretised in time and, at each time step, they are solved with the aid of a linearisation method. This requires to compute the directional averages that define $\hat{\mathbf{P}}_{\text{sc}}$, $\hat{\mathbf{K}}$, and $\partial \hat{W}_{\text{std}}/\partial Q$, along with their derivatives (such derivatives, indeed, appear in the linearisation scheme). In fact, the evaluation of these averages is accomplished by having recourse to the numerical procedure known as Spherical Design Algorithm (SDA) [63]. Since presenting the whole procedure is rather lengthy and out of the scope of our work, we show here only the construction of $\partial \hat{W}_{\text{std}}/\partial Q$ (see algorithm A1).

5.1 Remodelling in the absence of deformation

In this section, we solve (62) independently of deformation. Such a situation occurs when no load is applied to the tissue (i.e., $\mathbf{g}(t)$ is zero for all times), the pore pressure is null at all times and at all points of the tissue, and no external force (such as the gravitational force) is considered. Hence, the sample is assumed to lean on the support beneath and its lower surface can be assumed to be free of surface forces. In this case, the balance laws (50a) and (50b) are trivially satisfied, and the term $\partial \hat{W}_{\text{std}}/\partial Q$ vanishes identically, so that the remodelling equation (62) becomes

$$\Gamma \dot{Q} = \text{Div} [D_0 \mathbf{G}^{-1} \text{Grad } Q] - \frac{\partial \hat{W}_{\text{AC}}}{\partial Q}, \quad (67)$$

840 with

$$\frac{\partial \hat{W}_{AC}}{\partial Q}(\mathbf{G}, Q) = \mathcal{A}_0 \frac{\partial \hat{\mathcal{P}}}{\partial Q}(Q) = \frac{4\mathcal{A}_0}{(\pi/4)^4} Q \left(Q - \frac{\pi}{2} \right) \left(Q - \frac{\pi}{4} \right). \quad (68)$$

841 We solve now (67) with the BCs (45a)–(45c) and under the hypothesis that,
 842 at the initial time of observation, the fibre mean angle $Q(X, 0)$ is a random
 843 function of X . Hence, the tissue finds itself in a disordered configuration at the
 844 initial time. We make this assumption in order to show that the Allen-Cahn
 845 model, along with the BCs (45a)–(45c), is capable of describing a change of the
 846 tissue’s material symmetry, which converts from the disordered configuration
 847 towards the ordered configuration that renders it transversely isotropic.

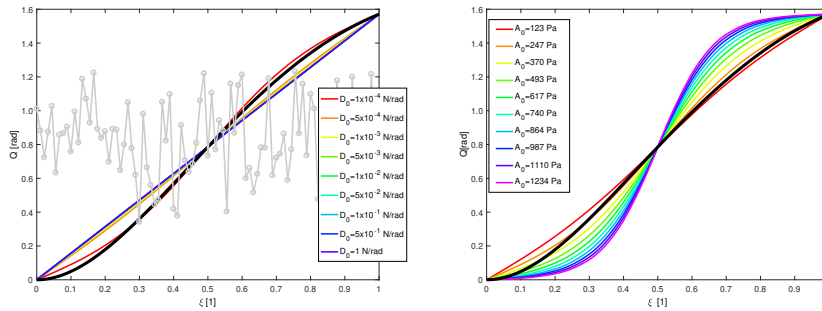


Fig. 3 Stationary profiles of the remodelling variable for different values of D_0 , with $\mathcal{A}_0 = 247$ Pa (a), and for different values of \mathcal{A}_0 , with $D_0 = 1.0 \cdot 10^{-4}$ N/rad (b). The grey circled curve in the plot on the left represents the initial profile of Q , which is set to be random.

848 The results of the initial-boundary value problem specified by (67), (68),
 849 and (45a)–(45c) are shown in Fig. 3 for varying values of the parameters D_0 (cf.
 850 Fig. 3a) and \mathcal{A}_0 (cf. Fig. 3b). Starting from a random profile (grey circled curve
 851 in Fig. 3a), which might represent the orientation of the fibres in an engineered
 852 tissue [64], $Q(X, t)$ evolves towards a stationary solution that is remnant of
 853 the histological profile reported in Fig. 2a. This behaviour is a consequence of
 854 the introduction of the Allen-Cahn energy density, \hat{W}_{AC} , whose two minimum
 855 configurations coincide with the boundary values imposed on Q , and manifests
 856 itself through the tendency of the remodelling variable to acquire a stationary
 857 solution interpolating between the imposed Dirichlet boundary conditions at
 858 the top (cf. (45a)) and at the bottom (cf. (45b)) of the sample. We remark that
 859 the free energy \hat{W}_{AC} generates a profile that is comparable with the histological
 860 one. In this respect we say that, in principle, the remodelling may occur also
 861 in the absence of deformation, and may be understood as a structural phase
 862 transition. Indeed, the system passes from a “phase” in which it appears to
 863 be disordered to a “phase” in which it is ordered in such a way that it is
 864 transversely isotropic. This loss, or *breaking*, of the system’s symmetries is due
 865 to the introduction of \hat{W}_{rem} .

866 5.2 Asymptotic “standard remodelling”

867 We launch a first set of simulations in which $\mathcal{R}_{\text{ext}} = 0$ and the free energy
 868 density is equal to the standard one only, i.e., $\hat{W} = \hat{W}_{\text{std}}$. In this case, the
 869 remodelling equation is given by (60) rather than (50c) and, as anticipated
 870 in Section (4.2), \hat{Q} tends towards zero for large values of t because (61) is re-
 871 spected asymptotically. To see why this occurs, it is necessary to determine I_4
 872 and construct the derivative $\partial\hat{W}_{\text{std}}/\partial Q$. The latter, in turn, requires to evalu-
 873 ate the directional averages reported in (49a) and, thus, to use the Spherical
 874 Design Algorithm [63]. Indeed, for a given \mathbf{C} , $\partial\hat{W}_{\text{std}}/\partial Q$, is approximated as

$$\begin{aligned}
 \frac{\partial\hat{W}_{\text{std}}}{\partial Q}(\mathbf{C}, Q) &= \frac{\Phi_{1s}}{\omega^2} \text{cov}(\Theta, \hat{W}_{1a}(\mathbf{C}, \hat{\mathbf{A}}(\Theta, \Phi))) \\
 &= \frac{\Phi_{1s}}{\omega^2} \langle (\Theta - \langle \Theta \rangle) \hat{W}_{1a}(\mathbf{C}, \hat{\mathbf{A}}(\Theta, \Phi)) \rangle \\
 &= \frac{\Phi_{1s}}{\omega^2} \int_0^{2\pi} \int_0^{\pi/2} (\Theta - \langle \Theta \rangle) \hat{W}_{1a}(\mathbf{C}, \hat{\mathbf{A}}(\Theta, \Phi)) \hat{\rho}(\Theta) \sin(\Theta) d\Theta d\Phi \\
 &\approx \frac{\Phi_{1s}}{\omega^2} \frac{2\pi}{N} \sum_{i=1}^m \sum_{j=1}^n (\Theta_i - \langle \Theta \rangle) \hat{W}_{1a}(\mathbf{C}, \mathbf{A}_{ij}) \hat{\rho}(\Theta_i), \tag{69}
 \end{aligned}$$

875 where $N = mn$ is the total number of quadrature points used for the numerical
 876 solution of the integral in (69), $\mathcal{J} \times \mathcal{J} \subset [0, \pi/2] \times [0, \pi]$ is the set of all quadrature
 877 points, and, for each $(\Theta_i, \Phi_j) \in \mathcal{J} \times \mathcal{J}$, we write $\mathbf{A}_{ij} = \mathbf{M}_{ij} \otimes \mathbf{M}_{ij}$ (*no* sum with
 878 respect to i and j), with $\mathbf{M}_{ij} = \hat{\mathbf{M}}(\Theta_i, \Phi_j)$. Hence, $\hat{W}_{1a}(\mathbf{C}, \mathbf{A}_{ij})$ is rewritten
 879 as

$$\hat{W}_{1a}(\mathbf{C}, \mathbf{A}_{ij}) = \mathcal{H}(I_4(\mathbf{C}, \mathbf{A}_{ij}) - 1) \frac{1}{2} c [I_4(\mathbf{C}, \mathbf{A}_{ij}) - 1]^2. \tag{70}$$

880 Note that \mathcal{J} and \mathcal{J} are sets of points suitably chosen in $[0, \pi/2]$ and $[0, 2\pi]$,
 881 respectively [40].

882 As prescribed in lines 21 and 22 of the pseudo-code of Algorithm A1, the
 883 summand of (69) with indices i and j contributes to $\partial\hat{W}_{\text{std}}/\partial Q$ only if $\hat{\rho}(\Theta_i)$
 884 is greater than a given threshold value, $\text{tol}_{\hat{\rho}}$, and $I_4(\mathbf{C}, \mathbf{A}_{ij}) > 1$. The first
 885 control is, in fact, on the probability density that a fibre is aligned along the
 886 direction specified by $(\Theta_i, \Phi_j) \in \mathcal{J} \times \mathcal{J}$. The second condition, instead, represents
 887 the algorithmic formulation of the Heaviside function in (70).

888 To have indications about these restrictions, we study the time evolution
 889 of $I_4(\mathbf{C}, \mathbf{A}_{ij})$ and $\hat{\rho}$ at two selected points of the sample, for different values
 890 of Θ . The results are reported in Fig. 4, where the black curves represent
 891 constant values for I_4 and $\hat{\rho}$, taken as reference (here, we choose $I_4^{(0)} = 1$
 892 and $\hat{\rho}^{(0)} = \text{tol}_{\hat{\rho}}$). Moreover, the point of coordinates $X_L = (0, 0, L/4)$ finds
 893 itself in the deep zone of the sample, in which the fibres tend to be parallel
 894 to the symmetry axis of the cylinder and, thus, perpendicular to the lower
 895 boundary (this corresponds to the bone-cartilage interface when the tissue is
 896 *in vivo*). The point of coordinates $X_U = (0, 0, 3L/4)$, instead, is situated in

Algorithm 1 –A5– Spherical Design Algorithm (SDA) for the evaluation of (49a) and (69) within the p th time step and the ℓ th linearisation iteration

```

1: procedure SDA
2:   for  $k = 1, \dots, M$  do ( $M$  is the number of grid nodes)
3:     Initialise  $\left(\frac{\partial \hat{W}_{\text{std}}}{\partial Q}\right)^{p\ell k} = 0$ , and  $\mathcal{Z}^{p\ell k} = 2\pi \int_0^{\pi/2} \hat{\gamma}^{p\ell k}(\Theta) \sin \Theta d\Theta = 0$  (partial sums)
4:     Load the point set  $\{(\Theta_i, \Phi_j)\}_{i,j=1}^{N=m_n} \subset \mathcal{J} \times \mathcal{J}$ 
5:     Load  $Q^{p\ell k} = Q^\ell(X_k, t_p)$  and  $\omega^k = \omega(\xi_k)$ 
6:     for  $i = 1, \dots, m$  do (inner cycle to evaluate the normalisation factor)
7:       Evaluate  $\hat{\gamma}^{p\ell k}(\Theta_i) = \exp\left(-\frac{(\Theta_i - Q^{p\ell k})^2}{2[\omega^k]^2}\right)$ 
8:        $\mathcal{Z}^{p\ell k} = \mathcal{Z}^{p\ell k} + \frac{2\pi}{N} \hat{\gamma}^{p\ell k}(\Theta_i)$ 
9:     end for
10:    Calculate  $\hat{\phi}^{p\ell k}(\Theta_i) = \frac{\hat{\gamma}^{p\ell k}(\Theta_i)}{\mathcal{Z}^{p\ell k}}$ ,  $i = 1, \dots, m$ 
11:    for  $i = 1, \dots, m$  do inner cycle to determine  $\langle \Theta \rangle^{p\ell k}$ 
12:      if  $\hat{\phi}^{p\ell k}(\Theta_i) > \text{tol}_\Psi$  then
13:         $\langle \Theta \rangle^{p\ell k} = \langle \Theta \rangle^{p\ell k} + \frac{2\pi}{N} \Theta_i \hat{\phi}^{p\ell k}(\Theta_i)$ 
14:      end if
15:    end for
16:    Given  $\mathbf{C}^{p\ell k}$ :
17:    for  $i = 1, \dots, m$  do
18:      for  $j = 1, \dots, n$  do
19:        Evaluate  $I_4(\mathbf{C}^{p\ell k}, \mathbf{A}_{ij}) = \mathbf{C}^{p\ell k} : \mathbf{A}_{ij}$ , and
20:         $\mathbf{A}_{ij} = \mathbf{M}_{ij} \otimes \mathbf{M}_{ij}$ , with  $\mathbf{M}_{ij} = \hat{\mathbf{M}}(\Theta_i, \Phi_j)$ 
21:        if  $\hat{\phi}^{p\ell k}(\Theta_i) > \text{tol}_\Psi$  then
22:          if  $I_4(\mathbf{C}^{p\ell k}, \mathbf{A}_{ij}) > 1$  then
23:            Evaluate
24:             $\mathcal{R}^{p\ell k}(\Theta_i, \Phi_j) = \frac{\Phi_{1s}(X_k)}{[\omega^k]^2} (\Theta_i - \langle \Theta \rangle) \frac{1}{2} c \left[ I_4(\mathbf{C}^{p\ell k}, \mathbf{A}_{ij}) - 1 \right]^2 \hat{\phi}^{p\ell k}(\Theta_i)$ 
25:             $\left(\frac{\partial \hat{W}_{\text{std}}}{\partial Q}\right)^{p\ell k} = \left(\frac{\partial \hat{W}_{\text{std}}}{\partial Q}\right)^{p\ell k} + \frac{2\pi}{N} \mathcal{R}^{p\ell k}(\Theta_i, \Phi_j)$ 
26:          end if
27:        end if
28:      end for
29:    end for
30:  end for
31: end procedure

```

897 the superficial zone, in which the fibres are parallel to the upper boundary
898 (which corresponds to the articular surface of the tissue *in vivo*).

899 Looking at the left column of Fig. 4, obtained for $X_U = (0, 0, 3L/4)$, we see
900 that the curves corresponding to $I_4(\mathbf{C}, \hat{\mathbf{A}}(2\pi/5, \Phi))$ and $I_4(\mathbf{C}, \hat{\mathbf{A}}(\pi/2, \Phi))$ are
901 above 1 for all the duration of the experiment, and tend to unity from above
902 for large times. Thus, at least in principle, the fibres aligned along $\hat{\mathbf{M}}(2\pi/5, \Phi)$
903 and $\hat{\mathbf{M}}(\pi/2, \Phi)$ contribute to $\partial \hat{W}_{\text{std}}/\partial Q$. However, the corresponding probabil-
904 ity densities become smaller than tol_Ψ as times goes by, thereby ruling out the
905 fibres oriented parallel to $\hat{\mathbf{M}}(2\pi/5, \Phi)$ and $\hat{\mathbf{M}}(\pi/2, \Phi)$. The curve correspond-
906 ing to $I_4(\mathbf{C}, \hat{\mathbf{A}}(\pi/3, \Phi))$ is above 1 up to a certain instant of time subsequent
907 T_{ramp} , and goes below 1 afterwards. Thus, the fibres aligned along $\hat{\mathbf{M}}(\pi/3, \Phi)$
908 do not contribute to $\partial \hat{W}_{\text{std}}/\partial Q$. Finally, all other curves are below 1 for all
909 the duration of the experiment and give, then, no contribution to (69).

910 The right column of Fig. 4, which refers to $X_L = (0, 0, L/4)$, shows that
911 the curve $I_4(\mathbf{C}, \hat{\mathbf{A}}(\pi/2, \Phi))$ is the only one that remains above 1, even though
912 it tends to unity for large values of t . The corresponding probability density,

913 however, goes below tol_Ψ after T_{ramp} , thereby nullifying the contribution to
 914 (69) stemming from the fibres oriented along $\hat{\mathbf{M}}(\pi/2, \Phi)$. In conclusion, Fig. 4
 915 indicates that, for sufficiently large values of t , $\partial\hat{W}_{\text{std}}/\partial Q$ tends towards zero
 916 because the deformation established in the sample and the values taken by the
 917 probability density switch off all the contributions of the sum (69).

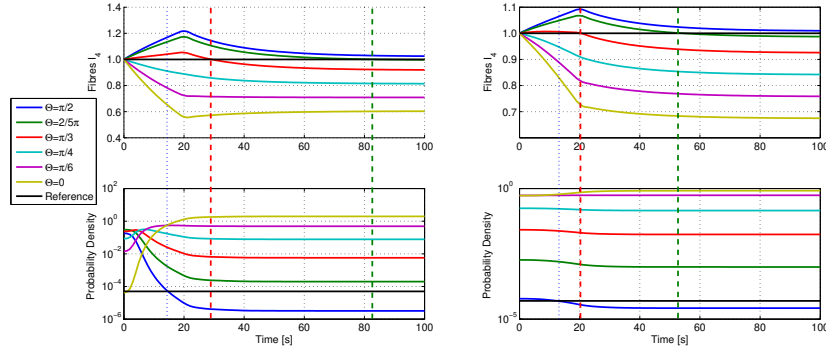


Fig. 4 Time evolution of $I_4(\mathbf{C}, \hat{\mathbf{A}}(\Theta, \Phi))$ and $\bar{\varphi}_X(\Theta)$ at $\Theta \in \mathcal{J} = \{0, \frac{\pi}{6}, \frac{\pi}{4}, \frac{\pi}{3}, \frac{2\pi}{5}, \frac{\pi}{2}\}$. Note that, for the computed deformation, $I_4(\mathbf{C}, \hat{\mathbf{A}}(\Theta, \Phi))$ is independent of Φ . The figures in the left column correspond to the point of coordinates $X_U = (0, 0, 3L/4)$; those in the right column to the point of coordinates $X_L = (0, 0, L/4)$.

918 5.3 “Standard” versus “non-standard” remodelling

919 It is worth to remark that, as long as it holds that $\hat{W} = \hat{W}_{\text{std}}$, the parameter Γ
 920 determines the stationary value of Q for a given loading time. Once this value
 921 is reached, if no additional compression is applied to the sample, then $\dot{Q} = 0$
 922 applies and no further evolution is observed. On the contrary, when the free
 923 energy density is given by $\hat{W} = \hat{W}_{\text{std}} + \hat{W}_{\text{rem}}$, with \hat{W}_{rem} specified in (31b),
 924 remodelling continues even when $\partial\hat{W}_{\text{std}}/\partial Q$ becomes negligibly small. This
 925 further evolution of the mean angle is induced by W_{rem} only. The described
 926 behaviour is represented in Figs. 5 and 6, where the evolution of Q and $-\Gamma\dot{Q}$
 927 over time is shown both in the case of “standard” and in the case of “non-
 928 standard” remodelling. Note that Figs. 5 and 6 are obtained by evaluating Q
 929 in $X_L = (0, 0, L/4)$ and $X_U = (0, 0, 3L/4)$, respectively.

930 “Standard” remodelling predicts that both $Q(X_L, t)$ and $Q(X_U, t)$ decrease
 931 monotonically towards asymptotically constant values (see Figs. 5a and 6a).
 932 This behaviour is consistent with the trend of $-\Gamma\dot{Q}$ shown in Figs. 5b and
 933 6b. Indeed, since $-\Gamma\dot{Q}(X_L, t)$ and $-\Gamma\dot{Q}(X_U, t)$ are both non-negative for all
 934 times, and Γ is strictly positive, the derivatives $\dot{Q}(X_L, t)$ and $\dot{Q}(X_U, t)$ are
 935 non-positive for all times. “Non-standard” remodelling, instead, destroys the

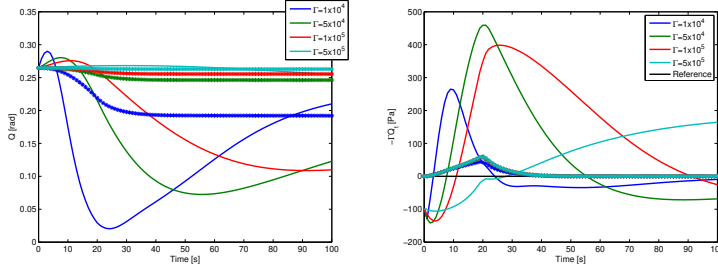


Fig. 5 (a): Time evolution of the mean angle Q . (b) Time evolution of $-\Gamma \dot{Q}$ (note that, in the label, the notation $Q_t \equiv \dot{Q}$ has been used). The dashed curves with asterisks refer to “standard” remodelling. The solid curves refer to “non-standard” remodelling for $a = 0$. All curves are obtained by evaluating both Q and $-\Gamma \dot{Q}$ in $X_L = (0, 0, L/4)$. The units of Γ are J s m^{-3} .

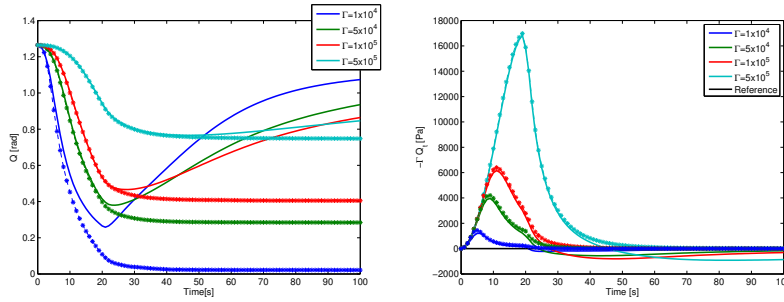


Fig. 6 (a): Time evolution of the mean angle Q . (b) Time evolution of $-\Gamma \dot{Q}$ (note that, in the label, the notation $Q_t \equiv \dot{Q}$ has been used). The dashed curves with asterisks refer to “standard” remodelling. The solid curves refer to “non-standard” remodelling for $a = 0$. All curves are obtained by evaluating both Q and $-\Gamma \dot{Q}$ in $X_U = (0, 0, 3L/4)$. The units of Γ are J s m^{-3} .

936 monotonicity of the curves $Q(X_L, t)$ and $Q(X_U, t)$, and slows down the rate
 937 by which they approach a stationary value.

938 From Fig. 5 we see that, in the case of “standard” remodelling, the variation
 939 of both $Q(X_L, t)$ and $-\Gamma \dot{Q}(X_L, t)$ is markedly smaller than it is in the case
 940 of “non-standard” remodelling. This behaviour is mainly due to the fact that
 941 the initial preferential direction of the fibres is close to the one that is parallel
 942 to the symmetry axis of the sample. Thus, for almost all fibres it holds $I_4 \leq 1$.
 943 In other words, the term $-\Gamma \dot{Q}$ in (60) (“standard” case) is much smaller than
 944 $-\Gamma \dot{Q}$ in (62) (“non-standard” case). In addition, we remark that, when the
 945 free energy density \hat{W}_{rem} is introduced, the quantity $-\Gamma \dot{Q}(X_L, t)$ is different
 946 from zero at $t = 0$ s. This is due to the fact that, at $t = 0$ s, \hat{W}_{std} is equal to
 947 the unessential constant α_0 , while \hat{W}_{rem} is non-trivial, because the gradient of
 948 Q is not null at $X = X_L$, and the value $Q(X_L, 0) \approx 0.265$ rad is sufficiently
 949 far away from the zeroes of $\partial \hat{W}_{\text{AC}} / \partial Q$ (at $t = 0$ s, they are $Q = 0$ rad, $Q =$
 950 $\pi/4$ rad, and $Q = \pi/2$ rad). For $t \geq 0$, $-\Gamma \dot{Q}(X_L, t)$ grows during the first
 951 instants of time of the loading ramp, thereby leading to a decrease of Q ,

952 and reaches an absolute maximum. Then, it goes below zero and tends again
 953 towards an asymptotic value. This trend, however, seems not to be followed for
 954 $\Gamma = 5.0 \cdot 10^5 \text{ J s m}^{-3}$ (see Fig. 5b), even though both $Q(X_L, t)$ and $-\Gamma Q(X_L, t)$
 955 converge to stationary values for sufficiently long times.

956 In contrast to what is observed in Fig. 5, we see in Fig. 6 that \hat{W}_{rem} does
 957 not affect appreciably the trend of the remodelling variable in the course of
 958 the loading ramp, i.e., for $t \in [0, T_{\text{ramp}}]$. For $t \geq T_{\text{ramp}}$, instead, the “standard”
 959 remodelling predicts a final value of Q that is constant in time and lower than
 960 the initial one, whereas \hat{W}_{rem} drives the growth of Q up to an asymptotic
 961 value that comes nearer to the initial one, with a rate of convergence ruled by
 962 Γ . We remark that, in “standard” remodelling, the parameter Γ is the only
 963 quantity that controls the stationary value of Q .

964 Finally, the strongest differences between the two compared models are at
 965 the final time of observation and in the relaxation times. Indeed, in the case of
 966 “non-standard” remodelling, the energetic contribution \hat{W}_{rem} is predominant
 967 in ruling the behaviour of the remodelling variable after the loading ramp,
 968 thus when $\partial \hat{W}_{\text{std}} / \partial Q$ tends towards zero, thereby mainly affecting the final
 969 state of the system.

In Fig. 7a, we report the axial profile of the circumferential component of
 the second Piola-Kirchhoff stress tensor *due to the fibres*, i.e.

$$\mathbf{S}_a = 2\Phi_{1s}(\partial \langle \hat{W}_{1a} \rangle / \partial \mathbf{C}),$$

970 evaluated at $T_{\text{end}} = 100 \text{ s}$. As expected, the occurrence of remodelling lowers
 971 the stress in the tissue in comparison with the case of no remodelling. We
 972 remark, however, that in the case of “non-standard” remodelling the stress
 973 behaviour is related to the choice of the boundary conditions imposed on Q .
 974 Indeed, the fact that in this work Q is constrained to be equal to $\pi/2 \text{ rad}$ at
 975 the upper boundary of the sample (see also Fig. 7b) produces in that zone a
 976 value of stress equal to the one obtained in the absence of remodelling. The
 977 “standard” remodelling, instead, for which no boundary conditions on Q are
 978 required, reduces the stress everywhere in the sample. The deviation is evident
 979 in the superficial (upper) zone of the sample, where the mean angle evolves
 980 the most (cf. Fig. 7b), and is barely visible in the deep (lower) zone, in which
 981 almost no remodelling occurs (see also the trend of Q shown in Fig. 7b).

982 In Fig. 8, we report the axial profile of the mean angle for $t \geq T_{\text{ramp}}$. In
 983 particular, by expressing Q as a function of the normalised axial coordinate
 984 and time, and recalling the parameter a introduced in (46), we compare the
 985 shape of $Q(\xi, t)$ computed for $a = 0$ with that obtained for $a \neq 0$. For $a = 0$
 986 (Fig. 8a), the plot of the mean angle tends to recover its initial shape for
 987 $t > T_{\text{ramp}}$. For $a \neq 0$ (Fig. 8b), instead, the curves obtained for $t > T_{\text{ramp}}$
 988 evolve in time while maintaining a shape similar to the curve determined
 989 for $t = T_{\text{ramp}}$. Since the profile of the mean angle is a representation of the
 990 pattern of fibre orientation in the sample, we conclude that, as expected, the
 991 introduction of a non-vanishing parameter a brings about structural changes
 992 that are more pronounced than in the case $a = 0$. This may be due to the fact
 993 that the condition $a \neq 0$ activates the term $\mathcal{A}_0 e^{\hat{a}w(\mathbf{C})Q} \hat{a}_W(\mathbf{C}) \hat{\mathcal{P}}(Q)$ on the

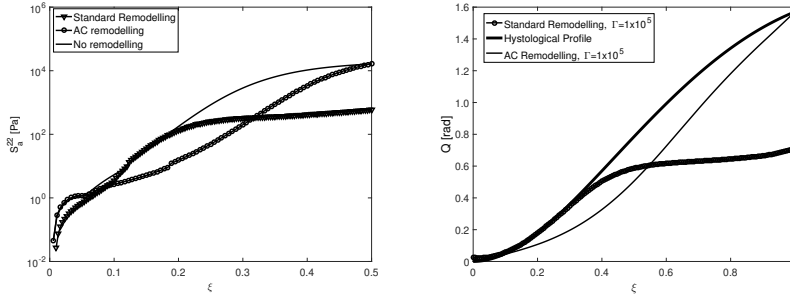


Fig. 7 (a) Circumferential component of the anisotropic part of the second Piola-Kirchhoff stress tensor, $(S_a)^{22}$ evaluated along the symmetry axis for $t = T_{\text{end}}$. (b) Axial profile of the mean angle for $t = T_{\text{end}}$. Note that the curves labelled with ‘‘AC remodelling’’ refer to the ‘‘non-standard’’ remodelling and are obtained with $a = 0$. The units of Γ are J s m^{-3} .

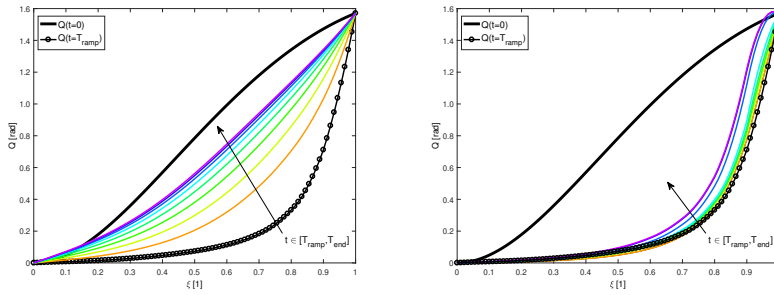


Fig. 8 Axial profile of Q for $t \geq T_{\text{ramp}}$ in the case $a = 0$ (a) and $a = 10^3$ (b). For both cases, we set $\Gamma = 1.0 \cdot 10^4 \text{ J s m}^{-3}$.

994 right-hand-side of (48b), which gives rise to an additional remodelling force.
 995 This, in turn, may be responsible for the marked change of the mean angle
 996 also in the deep zone of the tissue (i.e., for values of ξ closer to zero), where
 997 otherwise only small changes of the mean angle are observed for $a = 0$. Indeed,
 998 when a is set equal to zero, the right-hand-side of (48b) reduces to

$$\frac{\partial \hat{W}}{\partial Q} = \frac{\partial \hat{W}_{\text{std}}}{\partial Q} + \mathcal{A}_0 \frac{\partial \hat{\mathcal{P}}}{\partial Q}, \quad (71)$$

999 and, since $\partial \hat{W}_{\text{std}} / \partial Q$ goes to zero for large times, the remodelling force $\partial \hat{W} / \partial Q$
 1000 that remains active also in the limit of large t , i.e., $\mathcal{A}_0 \partial \hat{\mathcal{P}} / \partial Q$, is independent
 1001 of deformation. This means that, for $a = 0$, the remodelling becomes asymp-
 1002 totically decoupled from deformation.

1003 6 Summary of results and further research

1004 The remodelling considered in our work consists of the reorientation of the col-
 1005 lagen fibres of a fibre-reinforced, hydrated soft tissue (e.g. articular cartilage),

1006 in which the fibres are aligned according to a prescribed probability density.
 1007 The remodelling process is described through the spatiotemporal evolution of
 1008 the mean angle associated with the fibre probability density. The mean angle
 1009 is determined by solving the balance of generalised forces presented in (10), in
 1010 which the generalised forces \mathcal{R}_{ext} and \mathcal{R}_{int} are said to be external and internal
 1011 remodelling forces, respectively. The force \mathcal{R}_{int} is assigned constitutively. To
 1012 this end, and motivated by histological observations, we proposed a constitutive
 1013 theory based on the introduction of the remodelling free energy density
 1014 \hat{W}_{rem} . This takes the spatial resolution of the mean angle explicitly into ac-
 1015 count, and features the Allen-Cahn term \hat{W}_{AC} , whose minimum configurations
 1016 coincide with the mean angles at the lower and upper boundary of the sample.

1017 Our first result is that our model determines the histological profile of the
 1018 mean angle as the solution of a partial differential equation, rather than by
 1019 fitting experimental data (see Fig. 2). This result, however, follows also from
 1020 the choice of the boundary conditions, and a histologically based calibration
 1021 of the model parameters D_0 and \mathcal{A}_0 . We interpreted this result as the mani-
 1022 festation of a spontaneous symmetry breaking, which makes the system pass
 1023 from a randomly distributed to a non-randomly distributed fibre mean angle.

1024 A comparison between the theory proposed in this work with that of “stan-
 1025 dard” remodelling is reported in Figs. 5, 6, and 7, in which we highlighted the
 1026 influence of \hat{W}_{rem} on the evolution in space and time of the mean angle and
 1027 of the stress distribution within the considered sample of tissue.

1028 Finally, we studied the influence of the parameter a , which features in
 1029 the definition of $\hat{\alpha}_W$ (see (46)), on the spatiotemporal evolution of Q . We
 1030 remark that, for $a = 0$, the free energy density \hat{W}_{AC} becomes a function
 1031 of Q only, i.e., $\hat{W}_{\text{AC}}(Q) = \mathcal{A}_0/(\pi/4)^4 Q^2(Q - \pi/2)^2$, and is thus invariant
 1032 under the discrete symmetry transformation $Q \mapsto \pi/2 - Q$. Such symmetry
 1033 manifests itself through the shape of the curves in Fig. 8a. On the contrary,
 1034 for $a \neq 0$, \hat{W}_{AC} loses this discrete symmetry because of the coupling with
 1035 the deformation (see (28)). We conclude that our theory of remodelling is
 1036 capable of describing the histological profile of the mean angle as the result of
 1037 a spontaneous symmetry breaking, which occurs in the tissue independently on
 1038 deformation (perhaps, when the tissue is generated) and proposes to interpret
 1039 the coupling between the evolution of Q and the deformation as a further
 1040 symmetry breaking (this time, however, a non-spontaneous one).

1041 A last remark should be made in regards of the time scales involved in the
 1042 considered remodelling process. Such time scales, indeed, are dictated in this
 1043 work by the loading history imposed from the outside and, for this reason, they
 1044 may appear unnatural. In fact, they represent a situation that is different from
 1045 the more natural one in which the characteristic time scale of remodelling is
 1046 the result of the coupling of this phenomenon with other processes, like e.g.
 1047 growth, and with the deformations and stresses induced by those. Introducing
 1048 growth in the description of remodelling presented in this work, and therefore
 1049 determining the natural time scales of these phenomena, is one of the objectives
 1050 of our studies.

1051 Our long term goal is to employ the approach proposed in our work for
 1052 characterising the structural evolution of fibrous tissues also in pathological
 1053 situations. For example, collagen orientation in articular cartilage varies due
 1054 to several reasons: It has been observed that, in a damaged or aged tissue [65,
 1055 66], the fibre orientation is quite far from that in the healthy tissue. In Fig.
 1056 9, the numerical results obtained in an unconfined compression test have been
 1057 qualitatively compared with the experimental outcomes shown in [65]. The
 1058 horizontal lines in the experimental figures mark each of the three zones of
 1059 articular cartilage (deep, middle, superficial). We see that, in a stressed and
 1060 damaged tissue, these three zones sensibly change, and in particular the deep
 1061 zone becomes more extended along the depth of the tissue, while the middle
 1062 zone shifts towards the top. A similar axial distribution of the remodelling vari-
 1063 able can be obtained, by means of the remodelling law (62) presented in this
 1064 work, at the end of a loading ramp in an unconfined compression. Naturally,
 1065 this result should be enriched by accounting, for example, for the concurrent
 1066 mass changes of both the collagen and the matrix, and for the reorganisa-
 1067 tion of the cells surrounding the fibres during realistic (either physiological or
 1068 pathological) loading conditions borne by the tissue. Also this topic is subject
 1069 of our current investigations.

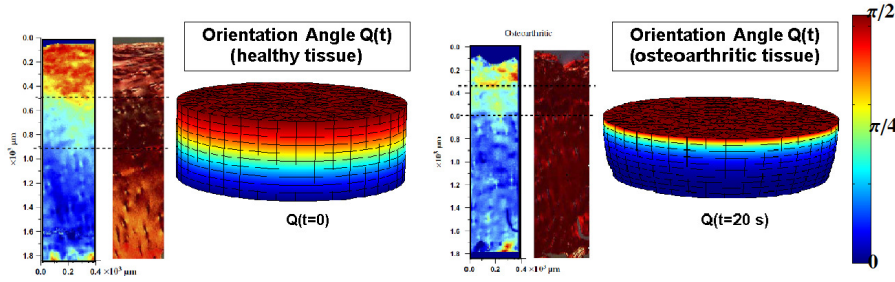


Fig. 9 Numerical simulations of an unconfined compression, in the unloaded initial configuration (left) and in the loaded condition at $t = T_{\text{ramp}}$ (deformed cylindrical shape on the right), have been qualitatively compared with the experimental results shown in [65]. The experimental observations (reported in the four columns featuring in the figure) correspond to a FT-IRIS image and a polarised light microscopy image (from left to right) directly taken from [65] (open access article). The four columns in the figure are reprinted from [65], Copyright (2005), with permission from Elsevier

1070 Appendix A

1071 To recall the relation between the operators in the physical space and those
 1072 in the reference configuration of a body, we select an open subset $\mathcal{C} \subset \mathcal{B}$ of
 1073 the reference configuration and we consider the map $\chi_t: \mathcal{C} \rightarrow \chi_t(\mathcal{C})$ that, at
 1074 each time t , embeds \mathcal{C} into the open subset $\chi_t(\mathcal{C}) \subset \mathcal{S}$ of the physical space
 1075 \mathcal{S} . Clearly, it applies that $\chi_t(X) = \chi(X, t)$ for all $X \in \mathcal{C}$ and for all t (cf.

Equation (1)). Then, let ${}^s f: \chi_t(\mathcal{C}) \rightarrow \mathbb{R}$ and ${}^s \mathbf{u}: \chi_t(\mathcal{C}) \rightarrow T\mathcal{S}$ be a scalar and a vector field, respectively, and let $f = {}^s f \circ \chi_t: \mathcal{C} \rightarrow \mathbb{R}$ and $\mathbf{u} = {}^s \mathbf{u} \circ \chi_t: \mathcal{C} \rightarrow T\mathcal{S}$ denote the counterparts of ${}^s f$ and ${}^s \mathbf{u}$ defined over \mathcal{C} . Thus, the identities $f(X) = {}^s f(\chi_t(X)) = {}^s f(x)$ and $\mathbf{u}(X) = {}^s \mathbf{u}(\chi_t(X)) = {}^s \mathbf{u}(x)$ hold true, with $x = \chi_t(X) \in \chi_t(\mathcal{C})$ and $X \in \mathcal{C}$. Hence, if all the partial derivatives of f and ${}^s f$ exist in \mathcal{C} and $\chi_t(\mathcal{C})$, respectively, enforcing the chain rule yields

$$\text{Grad } f = [\mathbf{F}^T \text{grad } {}^s f] \circ \chi_t \quad \Rightarrow \quad \text{grad } {}^s f = [\mathbf{F}^{-T} \text{Grad } f] \circ \chi_t^{-1}, \quad (72a)$$

$$\text{Grad } \mathbf{u} = [(\text{grad } {}^s \mathbf{u}) \circ \chi_t] \mathbf{F} \quad \Rightarrow \quad (\text{grad } {}^s \mathbf{u}) \circ \chi_t = (\text{Grad } \mathbf{u})(\mathbf{F}^{-1} \circ \chi_t). \quad (72b)$$

The divergence of ${}^s \mathbf{u}$ is given by

$$\begin{aligned} (\text{div } {}^s \mathbf{u}) \circ \chi_t &= \text{tr}[(\text{grad } {}^s \mathbf{u}) \circ \chi_t] \\ &= \text{tr}[(\text{Grad } \mathbf{u})(\mathbf{F}^{-1} \circ \chi_t)] = (\text{Grad } \mathbf{u}) : \mathbf{F}^{-T}. \end{aligned} \quad (73)$$

Note that in (72a), (72b), and (73) the explicit dependence of \mathbf{F} on time is omitted but understood, and that, in the definitions of f and \mathbf{u} , time t plays the role of a parameter.

Given a differentiable material vector field $\mathbf{U}: \mathcal{C} \rightarrow T\mathcal{B}$, the divergence of \mathbf{U} in \mathcal{C} reads

$$\text{Div } \mathbf{U} = \text{tr}[\text{Grad } \mathbf{U}]. \quad (74)$$

If ${}^s \mathbf{u}$ is the flux vector associated with some scalar physical quantity, then the material counterpart of ${}^s \mathbf{u}$ is defined through the Piola transformation $\mathbf{U} = J(\mathbf{F}^{-1} \circ \chi_t) \mathbf{u}$, with $\mathbf{u} = {}^s \mathbf{u} \circ \chi_t$, and the divergences $\text{div } {}^s \mathbf{u}$ and $\text{Div } \mathbf{U}$ are related through [41]

$$J(\text{div } {}^s \mathbf{u}) \circ \chi_t = \text{Div } \mathbf{U}. \quad (75)$$

In the sequel, the compositions with χ_t and χ_t^{-1} will be omitted for the sake of a lighter notation.

The definitions reported above can be generalised to the computation of the gradient and divergence of tensor fields of any order (see e.g. [41] for details). If, for example, ${}^s \mathbf{t}$ is a second-order tensor field defined over $\chi_t(\mathcal{C}) \subset \mathcal{S}$ and characterised by contravariant components, its gradient, $\text{grad } {}^s \mathbf{t}$, is a third-order tensor field with two contravariant indices (i.e., those corresponding to the first pair of indices) and one covariant index (i.e., that individuated by the direction along which the covariant differentiation is performed), while its divergence, $\text{div } {}^s \mathbf{t}$, is the unique vector field satisfying $\text{div}({}^s \mathbf{t}^T \cdot \mathbf{h}) = (\text{div } {}^s \mathbf{t}) \cdot \mathbf{h}$, for all constant spatial vectors \mathbf{h} . In components, $\text{div } {}^s \mathbf{t}$ reads $(\text{div } {}^s \mathbf{t})^a = ({}^s \mathbf{t})^{ab}_{;b}$, where the semicolon “;” stands for partial covariant differentiation.

Often, the notation $\text{grad } {}^s f$ and $\text{div } {}^s \mathbf{u}$ is replaced by $\text{grad } {}^s f \equiv \nabla {}^s f$ and $\text{div } {}^s \mathbf{u} \equiv \nabla \cdot {}^s \mathbf{u}$ (accordingly, for the material description, one writes $\text{Grad } f \equiv \nabla_{\mathbf{R}} f$ and $\text{Div } \mathbf{U} \equiv \nabla_{\mathbf{R}} \cdot \mathbf{U}$, the subscript “ \mathbf{R} ” meaning that the differentiation is done in the reference configuration). In this paper, however, for the sake of consistency with the notation adopted in previous works, we prefer to use the

1109 symbols “grad” and “div” for the operators in the physical space and “Grad”
 1110 and “Div” for the operators in the reference configuration. Moreover, in the
 1111 differential geometric approach that we follow, the symbol nabla, ∇ , is usually
 1112 reserved to a *connection*, i.e., a *covariant derivative*. While ∇ and grad could
 1113 be used interchangeably, the use of “ $\nabla \cdot$ ” for div becomes cumbersome as it
 1114 relies on the traditional abuse of notation according to which ∇ is a “vector”,
 1115 which does *not* fit with covariant differentiation.

1116 Appendix B

1117 Within a purely mechanical framework (i.e., in the absence of thermal effects),
 1118 and under the hypothesis that the mass densities of the solid and the fluid
 1119 phase are constant, the dissipation inequality, written per unit volume of the
 1120 tissue’s reference configuration, can be cast in the form

$$\begin{aligned} \mathfrak{D}_0 = & -\dot{W} + \mathbf{P}_s : \mathbf{g}\dot{\mathbf{F}} + \mathbf{P}_f : \mathbf{g} \text{Grad}\mathbf{v}_f - J\boldsymbol{\pi}_f \cdot \mathbf{w} \\ & + \mathcal{R}_{\text{int}}\dot{Q} + \text{Div}(-T\bar{\boldsymbol{\Omega}}^\eta) \geq 0. \end{aligned} \quad (76)$$

1121 Equation (76) is obtained by specialising the theoretical framework developed,
 1122 for example, by Hassanizadeh [67], Bennethum et al. [68], and Grillo et al. [22]
 1123 to the setting presented in our work. In the definition of \mathfrak{D}_0 , W is the overall
 1124 energy density of the solid phase, expressed per unit volume of the reference
 1125 configuration and defined in (31a), $\mathbf{P}_s : \mathbf{g}\dot{\mathbf{F}}$ and $\mathbf{P}_f : \mathbf{g} \text{Grad}\mathbf{v}_f$ are the internal
 1126 mechanical power densities produced by the agency of the first Piola-Kirchhoff
 1127 stress tensors \mathbf{P}_s and \mathbf{P}_f on $\dot{\mathbf{F}}$ and $\text{Grad}\mathbf{v}_f$, respectively, $J\boldsymbol{\pi}_f \cdot \mathbf{w}$ is the power
 1128 density related to the interaction force between the fluid and the solid phase,
 1129 i.e., $\boldsymbol{\pi}_f$, which is conjugate to the relative velocity $\mathbf{w} = \mathbf{v}_f - \mathbf{v}_s$, $\mathcal{R}_{\text{int}}\dot{Q}$ is the
 1130 internal power density associated with remodelling, T is absolute temperature,
 1131 and $\bar{\boldsymbol{\Omega}}^\eta$ is the entropy flux vector. We remark that, since thermal effects are
 1132 excluded from the present context, T is here understood as a constant reference
 1133 temperature, which provides $T\bar{\boldsymbol{\Omega}}^\eta$ with the physical units of energy flux vector.

1134 We notice that, in the Classical Thermodynamics of Irreversible Processes,
 1135 the entropy flux vector is usually defined by dividing the heat flux vector
 1136 by the absolute temperature [69]. Therefore, if this hypothesis is accepted,
 1137 there can be no entropy flux vector in a theory in which thermal effects —and,
 1138 consequently, the heat flux vector— are disregarded from the outset. However,
 1139 within a more general setting, the entropy flux vector of a thermodynamic
 1140 theory need not be related *a priori* to the heat flux vector [55]. In fact, this is
 1141 the case studied in our work, which is non-classical in the sense that the free
 1142 energy density of the solid phase depends on the gradient of the fibre mean
 1143 angle, Q , as well as on Q itself. Hence, if the approach outlined by Jamet
 1144 [55] is adopted, one might introduce the entropy flux vector $\bar{\boldsymbol{\Omega}}^\eta$ even in a
 1145 purely mechanical framework, in which, thus, the heat flux vector is absent,
 1146 and determine a constitutive representation for it. This is, in fact, the path
 1147 followed in our work.

1148 To show the calculations leading to the definitions of the terms reported
1149 in (30a)–(30d), i.e., \mathfrak{D}_I , \mathfrak{D}_{II} , \mathfrak{D}_{III} , and \mathfrak{D}_{IV} , we modify (76) as

$$\begin{aligned} \mathfrak{D} = \mathfrak{D}_0 + p \left[\Phi_s \mathbf{F}^{-T} : \dot{\mathbf{F}} + (J - \Phi_s) \mathbf{F}^{-T} : \text{Grad} \mathbf{v}_f \right. \\ \left. + (J \mathbf{g}^{-1} \text{grad} \phi_f) \cdot \boldsymbol{\omega} \right] \geq 0, \end{aligned} \quad (77)$$

1150 where p is pressure, and the sum of the terms in brackets expresses the mass
1151 balance law for the system as a whole, i.e.,

$$\Phi_s \mathbf{F}^{-T} : \dot{\mathbf{F}} + (J - \Phi_s) \mathbf{F}^{-T} : \text{Grad} \mathbf{v}_f + (J \mathbf{g}^{-1} \text{grad} \phi_f) \cdot \boldsymbol{\omega} = 0. \quad (78)$$

1152 We recall that (78) is obtained by adding together the mass balance laws for
1153 the solid and the fluid phase, which, in the case of constant mass densities,
1154 can be written as

$$D_s \phi_s + \phi_s \text{div} \mathbf{v}_s = 0, \quad (79a)$$

$$D_s \phi_f + (\text{grad} \phi_f) \boldsymbol{\omega} + \phi_f \text{div} \mathbf{v}_f = 0, \quad (79b)$$

1155 and computing the backward Piola transform of the result.

1156 In writing (77), the mass balance law of the mixture as a whole is treated
1157 as a constraint of the theory, and the pressure p is thus the Lagrange multiplier
1158 associated with it. Moreover, since the terms between brackets in (77) add up
1159 to zero, \mathfrak{D} and \mathfrak{D}_0 are numerically equal to each other, although they acquire a
1160 rather different meaning. For a discussion on the subject, the Reader is referred
1161 to [68].

1162 By substituting the expression of \mathfrak{D}_0 in (77), the dissipation inequality
1163 becomes

$$\begin{aligned} \mathfrak{D} = -\dot{W} + \left[\mathbf{P}_s + \Phi_s p \mathbf{g}^{-1} \mathbf{F}^{-T} \right] : \mathbf{g} \dot{\mathbf{F}} \\ + \left[\mathbf{P}_f + (J - \Phi_s) p \mathbf{g}^{-1} \mathbf{F}^{-T} \right] : \mathbf{g} \text{Grad} \mathbf{v}_f \\ - J [\boldsymbol{\pi}_f - p \mathbf{g}^{-1} \text{grad} \phi_f] \cdot \boldsymbol{\omega} \\ + \mathcal{R}_{\text{int}} \dot{Q} + \text{Div}(-T \bar{\boldsymbol{\Sigma}}^\eta) \geq 0. \end{aligned} \quad (80)$$

1164 Then, we expand the time derivative of W , thereby obtaining

$$\begin{aligned} \dot{W} &= \frac{\partial \hat{W}}{\partial \mathbf{C}} : \dot{\mathbf{C}} + \frac{\partial \hat{W}}{\partial Q} \dot{Q} + \frac{\partial \hat{W}}{\partial \text{Grad} Q} \overline{\text{Grad} \dot{Q}} \\ &= \frac{\partial \hat{W}}{\partial \mathbf{C}} : \dot{\mathbf{C}} + \frac{\partial \hat{W}}{\partial Q} \dot{Q} + \frac{\partial \hat{W}}{\partial \text{Grad} Q} \text{Grad} \dot{Q} \\ &= \mathbf{F} \left(2 \frac{\partial \hat{W}}{\partial \mathbf{C}} \right) : \mathbf{g} \dot{\mathbf{F}} + \text{Div} \left[\frac{\partial \hat{W}}{\partial \text{Grad} Q} \dot{Q} \right] \\ &\quad + \left[\frac{\partial \hat{W}}{\partial Q} - \text{Div} \left(\frac{\partial \hat{W}}{\partial \text{Grad} Q} \right) \right] \dot{Q}. \end{aligned} \quad (81)$$

1165 Finally, by replacing the right-hand-side of (81) into (80), and grouping to-
 1166 gether all the terms that multiply the same generalised velocity, we find

$$\begin{aligned}
 \mathfrak{D} = & \left\{ -\mathbf{F} \left(2 \frac{\partial \hat{W}}{\partial \mathbf{C}} \right) + \mathbf{P}_s + \Phi_s p \mathbf{g}^{-1} \mathbf{F}^{-\text{T}} \right\} : \mathbf{g} \dot{\mathbf{F}} \\
 & + \left\{ \mathbf{P}_f + (J - \Phi_s) p \mathbf{g}^{-1} \mathbf{F}^{-\text{T}} \right\} : \mathbf{g} \text{Grad} \mathbf{v}_f \\
 & - J [\boldsymbol{\pi}_f - p \mathbf{g}^{-1} \text{grad} \phi_f] \cdot \mathbf{w} \\
 & + \left\{ \mathcal{R}_{\text{int}} - \left[\frac{\partial \hat{W}}{\partial Q} - \text{Div} \left(\frac{\partial \hat{W}}{\partial \text{Grad} Q} \right) \right] \right\} \dot{Q} \\
 & + \text{Div} \left[- \frac{\partial \hat{W}}{\partial \text{Grad} Q} \dot{Q} - T \bar{\boldsymbol{\zeta}}^\eta \right] \geq 0. \tag{82}
 \end{aligned}$$

1167 Thus, the terms \mathfrak{D}_I , \mathfrak{D}_{II} , \mathfrak{D}_{III} , and \mathfrak{D}_{IV} can be identified by comparing (82)
 1168 with (30a)–(30d). In principle, \mathfrak{D}_I accounts for the dissipative stresses asso-
 1169 ciated with the solid and the fluid phase, respectively. However, since in our
 1170 work the solid phase is assumed to be hyperelastic, and the fluid is assumed
 1171 to be macroscopically inviscid, neither the solid nor the fluid phase feature
 1172 a dissipative stress. Hence, \mathfrak{D}_I must vanish identically. The term \mathfrak{D}_{II} is the
 1173 dissipation due to the solid-fluid interactions. In fact, the brackets multiplying
 1174 \mathbf{w} define the dissipative part of the interaction force density $\boldsymbol{\pi}_f$, which leads to
 1175 Darcy’s law. Analogously, \mathfrak{D}_{III} consists of the dissipation related to the process
 1176 of remodelling, and the coefficient of \dot{Q} determines the dissipative part of the
 1177 internal remodelling generalised force \mathcal{R}_{int} . Finally, \mathfrak{D}_{IV} is assumed to vanish
 1178 in the present context, thereby defining the entropy flux vector $\bar{\boldsymbol{\zeta}}^\eta$.

1179 We emphasise that the framework within which the dissipation inequality
 1180 is studied in our work is based on the hypothesis of validity of Darcy’s law for
 1181 the description of the fluid filtration velocity. Moreover, neither the dissipa-
 1182 tive effects related to the mixture viscosity [70] nor those connected with the
 1183 microstructure viscosity of the considered medium [70] are taken into account.
 1184 These, however, can be relevant in the poroelastic approach to bone structure
 1185 developed in [70]. In addition, for increasing magnitude of the tissue’s per-
 1186 meability, also a possible deviation from the flow regime predicted by Darcy’s
 1187 law can be appreciable. Indeed, when this is the case, the Brinkman correction
 1188 should be included into the model [70].

1189 **Acknowledgements** We would like to thank Dr. Lorenzo Tentarelli for useful discussions.

1190 In Memoriam

1191 In memory of our master, Prof. Gaetano Giaquinta (1945–2016), who inspired
 1192 this work back in 2004, by suggesting the use of the Ginzburg-Landau energy.

1193 Compliance with Ethical Standards

1194 The authors declare that they have no conflict of interest.
 1195

References

- 1196
1197
1198
1199
1200
1201
1202
1203
1204
1205
1206
1207
1208
1209
1210
1211
1212
1213
1214
1215
1216
1217
1218
1219
1220
1221
1222
1223
1224
1225
1226
1227
1228
1229
1230
1231
1232
1233
1234
1235
1236
1237
1238
1239
1240
1241
1242
1243
1244
1245
1246
1247
1248
1249
1250
1251
1. Cowin SC (2000) How is a tissue built? *J Biomech Engng* 122:553–569.
 2. Holzapfel GA, Gasser TC, Ogden RW (2000) A new constitutive framework for arterial wall mechanics and a comparative study of material models. *J Elast* 61:1–48
 3. Holzapfel GA, Gasser TC (2001) A viscoelastic model for fiber-reinforced composites at finite strains: continuum basis, computational aspects and applications. *Comput Methods Appl Mech Eng* 190:4379–4403
 4. Merodio J, Ogden RW (2005) Mechanical response of fiber-reinforced incompressible non-linearly elastic solids. *Int J Non-Linear Mech*,40:213–227
 5. Merodio J (2006) On constitutive equations for fiber-reinforced nonlinearly viscoelastic solids. *Mech Res Commun* 33:764–770
 6. deBotton G, Schmucl G (2009) Mechanics of composites with two families of finitely extensible fibers undergoing large deformations. *J Mech Phys Solids* 57:1165–1181
 7. Lanir Y (1983) Constitutive equations for fibrous connective tissues. *J Biomech* 16:1–12
 8. Gasser TC, Ogden RW, Holzapfel GA (2006) Hyperelastic modelling of arterial layers with distributed collagen fibre orientations. *J R Soc Interface* 3:15–35
 9. Federico S, Herzog W (2008) On the anisotropy and inhomogeneity of permeability in articular cartilage. *Biomech Model Mechanobiol* 7:367–378
 10. Federico S, Gasser TC (2010) Non-linear elasticity of biological tissues with statistical fibre orientation. *J R Soc Interface*, 7:955–966
 11. Menzel A (2005) Modelling of anisotropic growth in biological tissues. *Biomech Model Mechanobiol* 3:147–171
 12. Menzel A (2007) A fibre reorientation model for orthotropic multiplicative growth. Configurational driving stresses, kinematics-based reorientation and algorithmic aspects. *Biomech Model Mechanobiol* 6(5):303–320
 13. Maroudas A, Bullough P (1968) Permeability of articular cartilage. *Nature* 219:1260–1261
 14. Federico S, Herzog W (2008) Towards an analytical model of soft tissues. *J Biomech* 41:3309–3313
 15. Federico S, Herzog, W (2008) On the permeability of fibre-reinforced porous materials. *Int J Solids Struct* 45:2160–2172
 16. Federico S, Grillo A (2012) Elasticity and permeability of porous fibre-reinforced materials under large deformations. *Mech Mater* 44:58–71
 17. Aspden RM, Hukins DWL (1981) Collagen organization in articular cartilage, determined by X-ray diffraction, and its relationship to tissue function. *Proc R Soc Lond B Biol Sci* 212:299–304
 18. Mollenhauer J, Aurich M, Muehleman C, Khelashvili G, Irving TC (2003) X-ray diffraction of the molecular substructure of human articular cartilage. *Connect Tissue Res* 44:201–207
 19. Di Carlo A and Quiligotti S (2002) Growth and balance. *Mech Res Commun* 29:449–456
 20. Fung YC (1990) *Biomechanics. Motion, Flow, Stress, and Growth*. Springer-Verlag, New York, USA
 21. Taber LA (1995) *Biomechanics of growth, remodeling and morphogenesis*. ASME Appl Mech Rev 48:487–545
 22. Grillo A, Federico S, Wittum G (2012) Growth, mass transfer, and remodeling in fiber-reinforced, multi-constituent materials. *Int J Nonlinear Mech* 47:388–401
 23. Grillo A, Wittum G, Tomic A, Federico S (2015) Remodelling in statistically oriented fibre-reinforced materials and biological tissues. *Math Mech Solids* 20(9):1107–1129
 24. Ginzburg VL, Landau LD (1950) On the theory of superconductivity. *Zh. Eksp. Teor. Fiz.* 20:1064–1082 [published in English in: Landau LD Collected papers, Pergamon Press, Oxford, UK (1965) p. 546]
 25. Ginzburg VL (2003) On superconductivity and superfluidity. Nobel Lecture 96–127
 26. Allen SM, Cahn JW (1979) A macroscopic theory for antiphase boundary motion and its application to antiphase domain coarsening. *Acta Metall* 27:1085–1095
 27. Olsson T, Klarbring A (2008) Residual stresses in soft tissue as a consequence of growth and remodeling: application to an arterial geometry. *Eur J Mech A-Solid* 27:959–974

- 1252 28. Cermelli P, Fried E, Sellers S (2001) Configurational stress, yield and flow in rate-
1253 independent plasticity. *Proc R Soc Lond A* 457:1447–1467
- 1254 29. Barocas VH, Tranquillo RT (1997) An anisotropic biphasic theory of tissue-equivalent
1255 mechanics: The interplay among cell traction, fibrillar network deformation, fibril align-
1256 ment, and cell contact guidance. *J Biomech Eng* 119:137–145
- 1257 30. Kroon M (2010) A continuum mechanics framework and a constitutive model for re-
1258 modelling of collagen gels and collagenous tissues. *J Mech Phys Solids* 58:918–933
- 1259 31. Imatani S, Maugin GA (2002) A constitutive model for material growth and its appli-
1260 cation to three-dimensional finite element analysis. *Mech Res Comm* 29:477–483
- 1261 32. Driessen NJB, Peters GWM, Huyghe JM, Bouten CVC, Baaijens FPT (2003) Remod-
1262 elling of continuously distributed collagen fibres in soft connective tissues. *J Biomech*
1263 36(8):1151–1158
- 1264 33. Ohsumi TK, Flaherty JE, Evans MC, Barocas VH (2008) Three-dimensional simulation
1265 of anisotropic cell-driven collagen gel compaction. *Biomechan Model Mechanobiol* 7:53–
1266 62
- 1267 34. Schrieff AJ, Zeindlinger G, Pierce DM, Regitnig P, Holzapfel GA (2012) Determi-
1268 nation of the layer-specific distributed collagen fibre orientations in human thoracic and
1269 abdominal aortas and common iliac arteries. *J R Soc Interface* 9:1275–1286
- 1270 35. Gasser TC, Gallinetti S, Xing X, Forsell C, Swedenborg J, Roy J (2012) Spatial ori-
1271 entation of collagen fibers in the abdominal aortic aneurysm's wall and its relation to
1272 wall mechanics. *Acta Biomater* 8:3091–3103
- 1273 36. Tsamis A, Krawiec JT, Vorp DA (2013) Elastic and collagen fibre microstructure of
1274 the human aorta in ageing and disease: A review. *J R Soc Interface* 10(83):1–22
- 1275 37. Quiligotti S, Maugin GA, dell'Isola F (2003) An eshelbian approach to the nonlinear
1276 mechanics of constrained solid-fluid mixtures. *Acta Mech* 160:45–60
- 1277 38. Tomic A, Grillo A, Federico S (2014) Poroelastic materials reinforced by statistically
1278 oriented fibres - numerical implementation and application to articular cartilage. *IMA*
1279 *J Appl Math* 79:1027–1059
- 1280 39. Grillo A, Guaily A, Givero C, Federico S (2015) Non-linear model for compression
1281 tests on articular cartilage. *J Biomech Eng* 137:071004–1–071004–8
- 1282 40. Carfagna M, Grillo A (2017) The spherical design algorithm in the numerical sim-
1283 ulation of biological tissues with statistical fibre-reinforcement. *Comput Visual Sci*
1284 <https://doi.org/10.1007/s00791-017-0278-6>
- 1285 41. Marsden JE, Hughes TJR (1983) *Mathematical Foundations of Elasticity*. Dover Pub-
1286 lications, Inc., New York
- 1287 42. Baaijens F, Bouthen C, Driessen N (2010) Modeling collagen remodeling. *J Biomech*
1288 43:166–175
- 1289 43. Ateshian GA, Weiss JA Anisotropic hydraulic permeability under finite deformation. *J*
1290 *Biomech Eng* 132:111004–1–111004–7
- 1291 44. Rivlin RS, Ericksen JL (1955) Stress-deformation relations for isotropic materials. *J*
1292 *Rational Mech Anal* 4:323–425
- 1293 45. Liu I-S (1982) On representations of anisotropic invariants. *Int J Eng Sci* 20(10):1099–
1294 1109
- 1295 46. Holmes MH, Mow VC (1990) The nonlinear characteristics of soft gels and hydrated
1296 connective tissues in ultrafiltration. *J Biomech* 23:1145–1156
- 1297 47. Hill R (1963) Elastic properties of reinforced solids: some theoretical principles. *J Mech*
1298 *Phys Solids* 11:357–372
- 1299 48. Walpole LJ (1969) On the overall elastic moduli of composite materials. *J Mech Phys*
1300 *Solids* 17:235–251
- 1301 49. Weng GJ (1990) The theoretical connection between Mori-Tanaka's theory and the
1302 Hashin-Shtrikman-Walpole bounds. *Int J Eng Science* 28:1111–1120
- 1303 50. Alhasadi MF, Federico S (2017) Relation between Eshelby stress and Eshelby fourth-
1304 order tensor within an ellipsoidal inclusion. *Acta Mech* 228:1045–1069
- 1305 51. Eshelby JD (1957) The determination of the elastic field of an ellipsoidal inclusion, and
1306 related problems. *Proc R Soc Lond A* 241:376–396
- 1307 52. Almeida ES, Spilker RL (1998) Finite element formulations for hyperelastic transversely
1308 isotropic biphasic soft tissues. *Comput Methods Appl Mech Eng* 151:513–538
- 1309 53. Felsager B (1998) *Geometry, Particles, and Fields*. Springer, Heidelberg, Germany

- 1310 54. Federico S, Grillo A, La Rosa G, Giaquinta G, Herzog W (2005) A transversely isotropic,
1311 transversely homogeneous microstructural-statistical model of articular cartilage. *J*
1312 *Biomech* 38:2008–2018
- 1313 55. Jamet D (2001) Diffuse interface models in fluid mechanics. *Adv Water Resour*
1314 25(3):335–348
- 1315 56. Macklin P, Lowengrub J (2007) Nonlinear simulation of the effect of microenvironment
1316 on tumor growth. *J Theor Biol* 245:677–704
- 1317 57. Wise SM, Lowengrub JS, Frieboes HB, Cristini V (2008) Three-dimensional multispecies
1318 nonlinear tumor growth—I model and numerical method. *J Theor Biol* 253:524–543
- 1319 58. Cristini V, Li X, Lowengrub JS, Wise SM (2009) Nonlinear simulations of solid tumor
1320 growth using a mixture model: invasion and branching. *J Math Biol* 58:723–763
- 1321 59. Wu JZ, Herzog W (2000) Finite element simulation of location- and time-dependent
1322 mechanical behavior of chondrocytes in unconfined compression tests. *Ann Biomed Eng*
1323 28:318–330
- 1324 60. Mow VC, Holmes MH, Lai MW (1984) Fluid transport and mechanical properties of
1325 articular cartilage: a review. *J Biomech* 17:377–394
- 1326 61. Pins GD, Huang EK, Christiansen DL, Silver FH (1997) Effects of static axial strain on
1327 the tensile properties and failure mechanisms of self-assembled collagen fibers. *J Appl*
1328 *Polym Sci* 63(11):1429–1440
- 1329 62. Hariton I, deBotton G, Gasser TC, Holzapfel GA (2007) Stress-driven collagen fiber
1330 remodeling in arterial walls. *Biomech Model Mechanobiol* 6(3):163–175
- 1331 63. Hardin RH, Sloane NJA (1996) McLaren’s improved snub cube and other new spherical
1332 designs in three dimensions. *Discrete Comput Geom* 15:429–441
- 1333 64. Paetzold H, Goepfert C, Huber G, Hoenic E, Pörtner R, Schilling AF, Meenen NM,
1334 Morlock MM (2012) The development of the collagen fibre network in tissue-engineered
1335 cartilage constructs in vivo. engineered cartilage reorganises fibre network. *Eur Cell*
1336 *Mater* 23:209–221
- 1337 65. Bi X, Li G, Doty SB, Camacho NP (2005) A novel method for determination of collagen
1338 orientation in cartilage by Fourier transform infrared imaging spectroscopy (ft-iris.)
1339 *Osteoarthr Cartilage* 13:1050–1058
- 1340 66. Julkunen P, Harjula T, Iivarinen J, Marjanen J, Seppänen T, Närhi T, Arokoski J,
1341 Lammi MJ, Brama PA, Jurvelin JS, Helminen HJ (2009) Biomechanical, biochemical
1342 and structural correlations in immature and mature rabbit articular cartilage. *Osteoarthr*
1343 *Cartilage* 17(12):1628–1638
- 1344 67. Hassanizadeh SM (1986) Derivation of basic equations of mass transport in porous
1345 media. Part 2. Generalized Darcy’s and Fick’s laws. *Adv Water Resour* 9:208–222
- 1346 68. Bennethum LS, Murad MA, Cushman JH (2000) Macroscale thermodynamics and the
1347 chemical potential for swelling porous media. *Transport Porous Med* 39:187–225
- 1348 69. Mićunović MV (2009) Thermomechanics of Viscoplasticity — Fundamentals and Ap-
1349 plications. Springer, Heidelberg, Germany
- 1350 70. Giorgio I, Andreus U, Scerrato D, dell’Isola F (2016) A visco-poroelastic model of
1351 functional adaptation in bones reconstructed with bio-resorbable materials. *Biomech*
1352 *Model Mechanobiol* 15(5):1325–1343